

# Temporal Development of HF-Excited Langmuir and Ion Turbulence at Arecibo

F. T. Djuth · D. F. DuBois

Received: 15 July 2014 / Accepted: 10 January 2015 / Published online: 3 March 2015  
© Springer Science+Business Media Dordrecht 2015

**Abstract** The Arecibo high-power, high-frequency (HF) facility and 430 MHz radar are used to examine the temporal development of the HF-induced Langmuir and ion turbulences from 1 ms to many minutes after the turn-on of the HF beam in the  $F$  region. All HF observations begin in a smooth, stratified, stable plasma. “Cold start” HF transmissions are employed to avoid remnant irregularities from prior HF transmissions. HF-excited plasma line (HFPL) and ion line echoes are used to monitor the evolution of the turbulence. In the evening/nighttime the HFPL develops in three reproducible stages. Over time scales of 0 to 10–20 ms (possibly 40 ms), the smooth plasma conditions are maintained, and the results are consistent with theoretical models of the excitation of strong Langmuir turbulence near HF reflection. This entails the initiation of the so-called “caviton production cycle.” The turbulence from the parametric decay instability is detected at lower altitudes where the radar wave vector matches those of the HF-enhanced waves. The data suggests that the two processes coexist in the region in between. After  $\sim 40$  ms the “overshoot process” begins and consists of a downward extension of the HFPL from the HF reflection region to heights  $\sim 1.1$  km below followed by a retreat back to the reflection region. The whole overshoot process takes place over a time scale of  $\sim 3$  s. Thereafter the echo remains near HF reflection for 20–90 s after HF turn-on. The HFPL echo subsequently breaks up into patches because of the formation of large-scale electron density structures in the plasma. New kinetic models indicate that suprathermal electrons excited in the plasma by, for example, caviton burn-out serve to regulate plasma turbulence in the modified ionospheric volume.

**Keywords**  $F$  region ionospheric modification · Enhanced plasma lines · Suprathermal electrons · Strong Langmuir turbulence · Cavitons · Thermal self-focusing

---

F. T. Djuth (✉)  
Geospace Research, Inc., 525 South Douglas Street, El Segundo, CA 90245, USA  
e-mail: fdjuth@geospace-research.com

D. F. DuBois  
Lodestar Research, Corp., 2400 Central Avenue, Boulder, CO 80301, USA

## 1 Introduction

In this paper we seek to introduce new researchers to the processes by which Langmuir wave (LW) and ion wave turbulence is excited in the ionospheric  $F$  region above Arecibo Observatory (AO), Puerto Rico. We present Arecibo 430 MHz radar results obtained in the past to illustrate what is currently known about the excitation process and what is not. In addition, measurements are suggested to help resolve key outstanding issues in anticipation of the start-up of the new high-frequency (HF) modification facility at AO.

When viewing AO data it is important to realize that the HF facility was not static. The ionospheric modification capability at Arecibo changed three times between 1970 and 1998, and in 2015 it is expected to change one more time. This is reflected in the types of measurements that could be made. High-power, HF ( $\sim 3\text{--}8$  MHz) experiments were initiated at AO in 1970 with the aid of a log periodic antenna suspended above the incoherent scatter radar reflector dish (305 m in diameter). The highly sensitive 430 MHz radar at AO serves as the central diagnostic for nearly all HF ionospheric modification experiments. With this arrangement the reflector dish is used as the antenna for both the 430 MHz radar and the HF transmissions. On average  $\sim 45\text{--}70$  MW HF effective radiated power (ERP = antenna gain  $\times$  transmitted power) was radiated with this system depending on frequency. On-site HF experiments at AO ended in 1979, and a new HF facility was constructed at a site located approximately 17 km northeast of AO near the coastal town of Islote. The Islote facility HF antenna consisted of a  $4 \times 8$  array of inverted (downward firing) log periodic antennas, with the longest array dimension oriented in the geographic east–west direction. Initially this facility was thought to generate  $\sim 80$  MW ERP across a frequency band from 3.175 to 8.175 MHz. However, it later became clear that the ERP with transmission line losses was closer to  $\sim 40$  MW than  $\sim 80$  MW. The initial period of Islote facility operation extended from 1980 to 1994. From 1994 to May 1997 this facility along with the Arecibo radar were shut down for the installation of the Gregorian feed system at AO. The Gregorian feed greatly improved the measurement flexibility of all projects involving the Arecibo dish, including 430 MHz radar measurements. Also during this period, the Islote transmission lines were upgraded, and a “true” 80 MW ERP was subsequently available for HF experiments. The upgraded Islote facility began operations in June 1997 and the last experiments were performed in February 1998. Hurricane Georges destroyed the facility in September 1998. Since then there has been no HF facility at Arecibo. However, a new facility with an antenna consisting of six crossed dipoles near the surface of the Arecibo dish and a suspended cassegrain reflector is scheduled to start operations in early 2015. This new HF system will initially operate at two frequencies 5.1 MHz ( $\sim 100$  MW ERP,  $13^\circ$  full width half max beam width) and 8.175 MHz ( $\sim 230$  MW ERP,  $8.5^\circ$  full width half max beam width).

The motivation for the current paper is to recapture the state of the Arecibo HF ionospheric modification science as developed through 1998 and beyond. Emphasis is placed on the temporal evolution of resonantly excited Langmuir oscillations/waves and ion waves in the ionospheric  $F$  region. The Arecibo 430 MHz incoherent scatter radar is sensitive to only those LWs that propagate parallel to the 430 MHz radar wave vector  $\mathbf{k}$ , where  $k = 2\pi/\lambda = 4\pi/\lambda_o$ ,  $\lambda_o$  is the wavelength of the radar transmissions (70 cm), and the Bragg condition for backscatter results in  $\lambda = \frac{1}{2}\lambda_o = 35$  cm. LWs that freely propagate in the ionosphere have a frequency  $\omega_r \equiv 2\pi f_r$ , that can be expressed to second order as.

$$\omega_r^2 = \omega_{pe}^2 + \sin^2 \theta \omega_{ce}^2 + \frac{3k^2 \pm \kappa T_e}{m_e}, \quad (1)$$

where  $\omega_{pe} = (n_e e^2 / \epsilon_0 m_e)^{1/2}$  and  $\omega_{ce}$  are the electron plasma frequency and the electron cyclotron frequency, respectively;  $n_e$  is electron concentration,  $e$  is electron charge,  $\epsilon_0$  is the permittivity of free space,  $m_e$  is electron mass,  $\theta$  is the angle between the radar line-of-sight and the geomagnetic field  $\mathbf{B}$ ;  $k_{\pm} = 2\pi/c[f_o + (f_o \pm f_r)]$  is radar wavenumber corrected for wave propagation downward (+, upshifted Doppler) and upward (-, downshifted Doppler) (e.g., Showen 1979);  $f_o$  is the radar operating frequency;  $c$  is the speed of light;  $T_e$  is electron temperature; and Boltzmann’s constant is represented as  $\kappa$ . Radar echoes at  $430 \text{ MHz} + f_r$  are referred to as upshifted plasma lines, whereas those at  $430 \text{ MHz} - f_r$  are downshifted plasma lines. Most but not all LWs excited through resonant HF wave-plasma interactions follow the dispersion relationship in (1) as do freely propagating waves (free modes) generated by HF instability processes. More generally, HF-enhanced plasma lines (HFPLs) are located near  $430 \text{ MHz} \pm f_{HF}$  (HFPL+ and HFPL-), where  $f_{HF}$  is the modifying HF frequency. Similarly, the HF-enhanced ion line (HFIL) corresponds to enhancements in the standard incoherent “ion line” spectrum centered near 430 MHz (see e.g., Evans 1969). The ion-acoustic waves (IAWs) responsible for the ion line are constant velocity waves. As a result one has.

$$f_{ia}\lambda = V_{ia} = \text{ion acoustic phase velocity} = \sqrt{\frac{\kappa}{m_i}(T_e + 3T_i)} \tag{2}$$

where  $f_{ia}$  is the ion-acoustic frequency,  $m_i$  and  $T_i$  are the ion mass ( $\text{O}^+ = 16 \text{ amu}$ ) and ion temperature, respectively. A schematic illustration of the Arecibo incoherent scatter spectrum is presented in Fig. 1 along with nominal HFPL and HFIL enhancements. Except when the HF wave greatly elevates electron temperature  $T_e$  (e.g., Djuth et al. 1987b; Djuth 1989), the HF-enhanced ion waves are more heavily damped (via ion Landau damping) in the  $F$  region plasma than the corresponding LWs. As a result the HFPL backscattered power is usually 10–100 times greater than that of the HFIL.

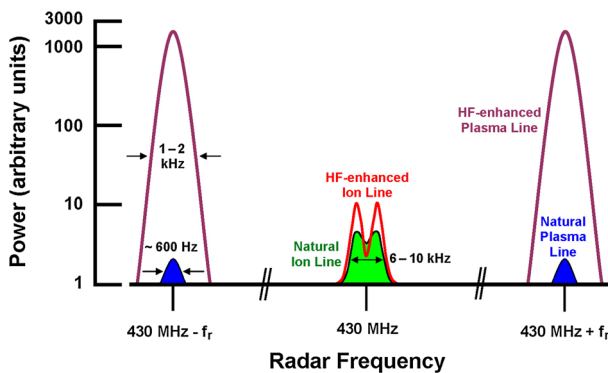


**Fig. 1** Schematic illustration of the natural incoherent scatter spectrum at Arecibo and HF-induced enhancements arising from the PDI. Note that the ordinate has a logarithmic scale. Only a single radar range cell in the  $F$  region is shown, and a homogeneous plasma is assumed. An electron temperature of 1,500 K and  $f_r = 5.1 \text{ MHz}$  were used to depict the natural plasma line signal. In addition, the radar beam is assumed to be directed vertically into the  $F$  region, and the angle between the beam and the geomagnetic field is taken to be the current value of  $44^\circ$ . The natural ion line spectrum corresponds to  $T_e/T_i \sim 1.5$ . The natural plasma line power includes the thermal enhancement generated by 1,500 K electrons, but not daytime photoelectrons. The photoelectron enhancement depends on time of day, the level of solar activity, the pointing angle of the radar beam, etc. However, the presence of photoelectrons will nominally increase the power of the natural plasma line in the above display by a factor of  $\sim 5$

There is a rich history of prior investigations in the area of HF ionospheric modification at AO, Puerto Rico beginning in the early 1970's and continuing until February 1998. Extensive studies of HF-induced plasma turbulence and artificially-produced, field-aligned irregularities (AFAIs), and beam/irregularity filamentation via thermal self-focusing have been performed at Arecibo. Characteristics of the HF enhanced plasma lines (HFPLs) observed with the Arecibo 430 MHz radar are described by Gordon et al. (1971), Carlson et al. (1972), Kantor (1974), Carlson and Duncan (1977), Muldrew and Showen (1977), Showen and Kim (1978), Morales et al. (1982), Duncan and Sheerin (1985), Djuth (1984), Fejer and Sulzer (1984), Fejer et al. (1985); Djuth et al. (1986), Birkmayer et al. (1986), Birkmayer and Hagfors (1986); Isham et al. (1987), Djuth et al. (1987a), Muldrew (1988), Sulzer et al. (1989), Sulzer and Fejer (1991), Cheung et al. (1989), Fejer et al. (1989), Djuth et al. (1990), Fejer et al. (1991), Cheung et al. (1992), Isham and Hagfors (1993), Sulzer and Fejer (1994), Cheung et al. (2001) and others. Properties of AFAIs observed at Arecibo are discussed by Lee and Fejer (1978), Frey and Gordon (1982), Lee and Kuo (1983), Basu et al. (1983), Coster et al. (1985), Noble et al. (1987), Noble and Djuth (1990), and Stocker et al. (1992). Investigations of horizontally-stratified irregularities in the Arecibo F region are limited to a single study performed by Fejer et al. (1984). Much theoretical work on the topic of HF-induced Langmuir turbulence was performed in the late 1960's, 1970's and 1980's and 1990's (e.g., DuBois and Goldman 1967; Fejer and Kuo 1973; Perkins 1974; Perkins et al. 1974; Nicholson and Goldman 1978; Muldrew 1978a, Muldrew 1978b; Fejer 1979; Weatherall et al. 1982; Sheerin et al. 1982; Kuo et al. 1983; Nicholson et al. 1984; Payne et al. 1984; Muldrew 1985; Doolen et al. 1985; Das et al. 1985; Russell et al. 1986; Muldrew 1986; Kuo et al. 1987; DuBois et al. 1988, 1990, 1991, 1992, 1993a, 1993b, 1995, 2001, hereafter DuBois et al.; Fejer 1988; Muldrew 1988; Russell et al. 1988; Payne et al. 1989; Kuo and Lee 1990; Kuo and Lee 1992; Muldrew 1992; Kuo et al. 1993; Lee et al. 1997; Kuo and Lee 1999, and others). Finally, stimulated electromagnetic emissions (SEE) were observed by Thidé et al. (1989) and Thidé (1990), and the evolution of Langmuir turbulence and SEE were simultaneously examined by Thidé et al. (1995). The current state of our understanding of HF-induced plasma turbulence at Arecibo is presented below. It serves as a reference point for future experiments to be conducted with the new Arecibo HF facility.

## 2 Early Time Development of the Arecibo HFPL

The HFPLs initially detected in the F region above Arecibo (e.g., Kantor 1974) were attributed to the parametric decay instability (PDI) (DuBois and Goldman 1965; Silin 1965). In addition, the data presented by Kantor (1974) suggested that the associated purely growing mode (Nishikawa 1968a, b) was also present in the plasma. The purely growing mode is also referred to as the oscillating two stream instability (OTSI) or the subsonic modulational instability. The PDI involves the parametric decay of the very long wavelength HF wave ( $\sim 30\text{--}100$  m) into a shorter-wavelength ( $\sim 0.1\text{--}1$  m) LW and an oppositely directed IAW having the same wavelength. In a smooth, stratified, stable ionospheric plasma () in the absence of HF-induced  $n_e$  irregularities the PDI is excited over a region bracketed by altitudes  $\sim 500$  m below HF reflection and heights above the upper hybrid resonance depending on the  $n_e$  vertical scale length  $H \equiv n_o / [dn_e(z)/dz]$ , where  $n_e(z)$  is electron concentration as a function of altitude  $z$ , and  $n_o$  is the electron concentration at the altitude of interest. However, a radar detects the PDI only at the altitude where wavenumber matching conditions are satisfied. The frequency matching condition



for the PDI demands that the frequency of the daughter LW be less than  $\omega_{HF} \equiv 2\pi f_{HF}$ , whereas the dispersion relation in the OTSI regime demands, for the fastest growing mode, that the LW frequency be slightly greater than  $\omega_{HF}$ . Since  $\omega_{HF}$  is greater than the local electron plasma frequency at altitudes below reflection the PDI is generally favored in the under-dense region, while the OTSI can exist even in the over-dense region where the HF wave is evanescent. These parametric instabilities, predicted from the linearization of the dynamical equations, provide a very incomplete understanding of HF-induced turbulence near reflection. These instabilities are predicted to grow exponentially in time (and space) with sub millisecond e-folding times. At the longer times usually observed after HF turn-on they would have grown to unphysically high levels. The theoretical challenge is to predict longer-time, nonlinear, saturation levels of the instabilities which are observed by radar measurements. Early work on the saturation of the PDI assumed that a nonlinear ion-Landau damping process can also be described as the Langmuir decay instability (LDI): the parametric decay of the primary PDI LW into an oppositely going LW and a (strongly Landau damped) ion acoustic wave (DuBois and Goldman 1967). This creates a cascade of daughter LWs (see e.g., DuBois and Goldman 1967, 1972; Valeo et al. 1972; Kruer and Valeo 1973; Fejer and Kuo 1973).

The PDI and OTSI are illustrated diagrammatically in Fig. 2. The OTSI with its zero frequency shift waves occurs at the altitude where the LW frequency at radar observed wavelength is only slightly greater than  $\omega_{HF}$  for weak HF power levels not in the strongly nonlinear regime (e.g., Sprague and Fejer 1995). This is to say that the OTSI waves are not exactly on the linear dispersion curve in (1). If the OTSI is strongly driven in a Smooth, Stratified, Stable, Plasma (SSSP) near the point of reflection, it can directly generate

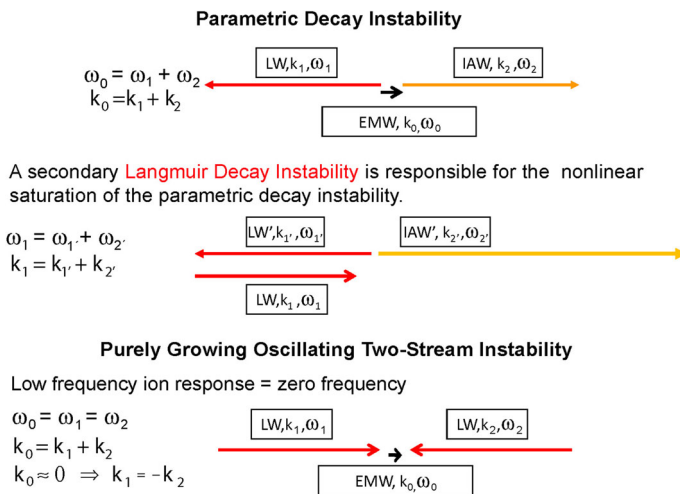


**Fig. 2** Illustration of the PDI instability process at the top and the purely growing OTSI at the bottom. The PDI entails the decay of the HF electromagnetic wave (EMW) wave into a LW and an oppositely directed IAW. The PDI saturates by the generation of a LW cascade; each peak of which is separated by  $\sim 2f_{ia}$ ; these daughter waves have frequencies less than the EMW and are the result of a nonlinear ion Landau process. However, the PDI cascade is ultimately terminated by the excitation of “caviton collapse.” The purely growing OTSI produces zero frequency ion fluctuations along with LWs having the same frequency as the EMW. This instability may appropriately be thought of as a five-wave process wherein the EMW decays into two oppositely directed LWs and two frequency-shifted ion acoustic waves of zero frequency. This instability, if strongly excited, can lead directly to the generation of “cavitons.”

“cavitons” (Doolen et al. 1983). (Cavitons are discussed in detail below.) This is a nonlinear effect that can obscure the linear signature of the OTSI. For example, one does not see any OTSI lines at  $430 \text{ MHz} \pm f_{\text{HF}}$  at early times (first 5–10 ms) in altitude–resolved SSSP HFPL data at Arecibo. The observations of HFPL peak(s) near  $430 \text{ MHz} \pm f_{\text{HF}}$  by Kantor (1974) were not made in an SSSP. Rather, these experiments were conducted in a plasma pre-conditioned by long periods of HF transmissions, and thus HF-induced irregularities that are highly striated along  $\mathbf{B}$  were almost certainly present in the plasma. The AFAs generate electron concentration ducts (e.g., Muldrew 1978a) that significantly alter LW propagation and greatly complicate the interpretation of the results in terms of parametric instability theory.

The linear and nonlinear physics of the HF induced turbulence appear to be well described in the SSSP regime by the extended Zakharov model (Zakharov 1972). For an early application of the extended model see Nicholson and Goldman (1978). This model relies on the separation of time scales between the Langmuir oscillations and the HF wave, both with frequencies near the electron plasma frequency and the low frequency electron and ion density fluctuations such as the IAWs. Two coupled, nonlinear, partial differential, evolution equations couple these disparate time scales: an equation for the frequency envelope of the longitudinal Langmuir electric field and an equation of evolution of the low frequency density fluctuations. The model has predicted many observed phenomena under SSSP conditions and can be derived directly from the Vlasov–Maxwell equations (DuBois et al. 1995). The model has also been validated by comparison with fully kinetic simulation models. The equations are solved numerically by split-step spectral techniques.

## 2.1 Wave-Plasma Theory

In the mid to late 1980’s, it became clear that many physical explanations that once seemed well-settled were seriously deficient. Nowhere is this more evident than in studies of resonant Langmuir turbulence with the Arecibo 430 MHz radar. The combination of greatly improved experimental techniques (e.g., Sulzer 1986a) together with a variety of new theoretical studies led to changes in the way resonant interactions near the point of O-mode reflection are studied and interpreted. Investigations of HF-induced LW/ion wave turbulence at early times after turn-on of the HF beam yielded many interesting results that reinforced the idea that our understanding of the wave-plasma interaction is far less than complete. Previous experimental investigations at Arecibo, Puerto Rico indicate that LWs detected with the 430 MHz incoherent scatter radar can occur near the point of O-mode wave reflection (Duncan and Sheerin 1985). This observation together with LW spectral data acquired at Arecibo (Djuth et al. 1986), new spectral predictions for SLT by DuBois et al. (1988), and observations of these predictions by Cheung et al. (1989) led to the realization that radar measurements of initially excited Langmuir oscillations are consistent with the extended Zakharov model calculations for Langmuir-ion sound wave interaction when nonlinearities in the plasma are large. The generalized concept of strong Langmuir turbulence (SLT) was originally put forth by DuBois et al. (1988). SLT is expected to be excited near the critical layer where  $f_{pe} = f_{\text{HF}}$ . Under conditions of SLT a significant fraction of the power in the HF density oscillations is contained within highly localized states termed “cavitons.”

Cavitons are localized states of Langmuir oscillations. The longitudinal electric field envelope of the Langmuir field is trapped in a local depression in the electron density, or cavity, thus the name “caviton.” When the trapped Langmuir field is resolved in spatial Fourier modes the frequencies of these modes of the localized state lie below the free LW dispersion curve (1); usually even below the local electron plasma frequency. Therefore

these states cannot be represented as a wave packet of free LWs; cavitons are an emergent nonlinear phenomenon. The localized LW electric field exerts a ponderomotive force which tends to reduce the local electron density which in turn localizes the field even more and lowers the frequencies further below the electron plasma frequency. The structure tends to collapse to smaller scales as first predicted by Zakharov (1972). The details of the collapse process depend on the spatial dimension of the theory or simulation and the method of driving. As the spatial scale decreases, and higher wave numbers are excited in the Fourier spectrum, the Langmuir electric field is quenched by a form of collisionless Landau damping. This leaves behind a density cavity with no trapped electric field, a result called “burn-out”. The burnt out density cavities can then be the nucleation centers for new cavitons with localized electric fields. The burn out process results in the acceleration of supra thermal electrons. The caviton production cycle is illustrated in Fig. 3. As cavitons collapse they radiate free LWs, often called “free modes”, which obey the dispersion relation (1), and they also radiate free IAWs obeying (2). Therefore the HFPL + radar spectra, from HF excitation under SSSP conditions, near reflection density consists of an up-shifted free mode lying on the dispersion curve (1) above the HF frequency, which therefore cannot be due to the PDI, and an additional down-shifted “collapse continuum” lying near and below the local electron plasma frequency. At this altitude, for SSSP conditions, this continuum also cannot be the result of PDI. These strong turbulence features, predicted by DuBois et al. (1988), were observed by Cheung et al. (1989), and later recognized to be the “displaced features” first observed by Djuth et al. (1986)

DuBois et al. (1990) provide an extensive discussion of SLT excited near the point of critical density during HF ionospheric modification experiments. DuBois et al. (1991) extend their caviton studies to include the pumping of the plasma by high-power HF waves at subcritical electron densities. They conclude that truncated parametric decay cascades coexist with caviton collapse events in the subcritical zone below radio wave reflection. In addition, a newly-predicted feature in the ion fluctuation spectrum at zero frequency is identified and attributed to caviton collapse. The subcritical concepts are further examined

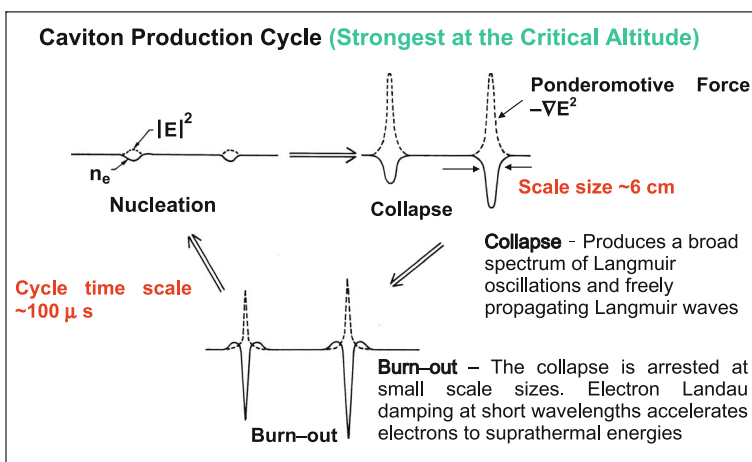


**Fig. 3** Schematic illustration of the caviton production cycle obtained from simulations based on modified Zakharov model equations (e.g., DuBois et al. 1990; DuBois et al. 1993a, b; Sanbonmatsu et al. 2000a, b). The nominal  $F$  region caviton scale size and cycle time are shown in red. (Color figure online)

in a resonance broadening study of weak turbulence by Hanssen (1991). Resonance broadening takes into account the purely nonlinear damping term that arises because electron orbits are perturbed in the presence of a pump electric field. He concludes that this effect is only important for high frequency radars such as the 933 MHz radar at EISCAT. Work aimed at numerically testing the validity of the weak turbulence approximation (WTA) in ionospheric modification experiments was performed by Hanssen et al. (1992). They compare solutions of a WTA derived from a 1-D driven and damped Zakharov system of equations (ZSE) with the same full ZSE. The number of PDI cascades apparent in the WTA is greater than that predicted by the full ZSE. At high pump intensities a truncation of the WTA cascades sets in, with subsequent filling of the bands between the cascades. The truncation of the cascade is apparently the result of cavitons nucleated in density depressions resulting from the interference of IAWs produced by early steps of the LDI cascade (e.g., Russell et al. 1999).

Sprague and Fejer (1995) also examined the WTA with emphasis on the OTSI using one-dimensional simulations based on the Zakharov equations. They address the issue of simultaneous excitation of parametric decay cascades and the OTSI. This is motivated by the lack of a convincing explanation for the OTSI feature in the Arecibo HFPL spectrum (e.g., Sulzer et al. 1984, 1989; Fejer et al. 1991) based on previous simulations of caviton dynamics. Sprague and Fejer found that low enough HF pump levels can support both parametric decay cascades and the OTSI feature. They indicate that the OTSI thus manifests itself in two different ways in ionospheric modification experiments; the near-linear case studied in their paper and the strongly nonlinear case where the OTSI can lead directly to the generation of cavitons.

The SLT theory was subsequently refined to include direct applications to HF ionospheric modification experiments such as the coexistence of the PDI and SLT at sub-critical levels and the signature of cavitons in the HF enhanced ion line spectrum DuBois et al. (1993a, 1993b, 1995). In this time frame SLT was also examined by Newman et al. (1990) using a particle-in-cell simulation, and Wang et al. (1994) investigated small 1D systems in the cavitation regime using the Vlasov approach. The diverse theoretical approaches yielded similar SLT results. In the work of Helmersen and Mjølhus (1994) Langmuir turbulence excited in HF experiments was studied with a model that treats the low-frequency ion dynamics using a linearized kinetic description while retaining the usual high frequency Zakharov equation describing the electron dynamics. Results from this model were compared with those previously obtained from quasi-fluid Zakharov models. The two types of models were found to be in good qualitative agreement. Wang et al. (1997) performed more extensive 1D Vlasov simulations than Wang et al. (1994) and included both the caviton regime and the regime where the LDI in Fig. 2 coexists with cavitons. This work provided important insight into the generation of suprathermal electrons during caviton burn-out. Methods for SLT and simulations have also been compared. A quantitative 1D comparison of reduced-description particle-in-cell and quasilinear-Zakharov (QLZ) models was made by Sanbonmatsu et al. (2000a), and the effect of kinetic processes on Langmuir turbulence including both cavitation and LDI cascades was assessed in Sanbonmatsu et al. (2000a). Suprathermal electron fluxes and electron velocity distribution functions were not investigated in this work. However, the work of Sanbonmatsu et al. (2000a, b) showed that particle effects (e.g., Cerenkov emissions by HF-induced suprathermal electrons) could be reproduced extremely well with the 1D QLZ model. DuBois et al. (2001) discuss the key theoretical work presented above within the context of HF ionospheric modification experiments conducted at Arecibo.

In all of the above simulation methods, the spatial size of the simulation domain is much less than the physical size of the modified ionospheric volume. Two- and three-dimensional kinetic modeling is the next step necessary to describe the ionospheric modification process in a more realistic manner. Kinetic simulations must account for energetic electrons entering and leaving the physical size of the heated region. The mean free path of the suprathermal electrons is much larger than the height extent of the HF modified volume. As a result, microscopic and macroscopic spatial scales must be tied together in a kinetic simulation of ionospheric wave-plasma interactions.

## 2.2 Radar Observations

A series of controlled experiments in the evening/nighttime  $F$  region at Arecibo (Fejer et al. 1991; Cheung et al. 1992; Sulzer and Fejer 1994; Cheung et al. 2001) revealed that the initial HF beam-plasma interaction in an SSSP in the absence of HF-induced irregularities was completely consistent with the SLT/LDI theory of DuBois et al. At the maximum power level available at Arecibo ( $\sim 40$  MW ERP prior to the HF facility upgrade), the predicted characteristics of SLT/LDI were observed for  $\sim 10$  ms following HF turn-on (Sulzer and Fejer 1994). Subsequent SLT/LDI experiments were performed with the HF facility at Tromsø, Norway to take advantage of the fact that the European Incoherent Scatter Radar (EISCAT) can be pointed nearly parallel to the HF pump electric field at the critical layer. This is not the case at Arecibo. The modal energy spectrum can be expressed as:

$$k^2 \langle |E(k_x, k_z)|^2 \rangle, \quad (3)$$

where  $k$  is wavenumber and  $k_x$  and  $k_z$  are the components in the horizontal and vertical directions, and  $E$  is wave electric field. Equation (3) represents all of the excited Langmuir oscillations including those generated by the PDI and is greatest when the  $\mathbf{k}$  vector diagnosed by the radar is closely aligned with the HF electric field near the critical level. Detailed simulations of the modal spectrum in the ionosphere are found in the work of DuBois et al. (2001). It is important to note that the PDI occurs over a continuous range of altitudes, but because radars have a fixed  $\mathbf{k}$ , the PDI waves and associated cascade waves are present only at ranges where the radar  $\mathbf{k}$  matches the  $\mathbf{k}$  of the instability waves. The electric field of the modifying HF wave having O-mode polarization is transformed into linear polarization parallel to the geomagnetic field  $\mathbf{B}$  in the vicinity of HF reflection. This has the added advantage of reducing electron Landau damping of the excited Langmuir oscillations, which is smallest parallel to  $\mathbf{B}$ . For a given  $n_e$  vertical scale length  $H$ , the transformation to linear polarization begins at a lower altitude at Arecibo than at Tromsø because of the smaller  $\sim 44^\circ$  geomagnetic dip angle at Arecibo. This is fortuitous for Arecibo because at the diagnostic  $k$  value ( $\sim 18 \text{ m}^{-1}$ ) the PDI is detected significantly below the critical level in an SSSP (depending on  $H$ ), whereas at Tromsø the 224 MHz radar ( $k \sim 9.4 \text{ m}^{-1}$ ) diagnoses the PDI at altitudes much closer to the point of HF reflection. At Arecibo the nominal radar viewing angles relative to the HF electric field at the critical level range from  $\sim 44^\circ$  to  $46^\circ$  depending on radar steering angle, whereas for experiments at Tromsø they are  $\sim 6^\circ$  to  $12^\circ$ . Thus the modal energy viewed by the Tromsø radar is much greater than that of Arecibo. However, this is in large part offset by the huge sensitivity of the Arecibo radar.

SLT experiments conducted at Tromsø include those described by Isham et al. (1999) Rietveld et al. (2000), Djuth et al. (2004). The HFPL/HFIL spectra are well-ordered in

altitude and the results confirmed the presence of all key HFPL/HFIL features predicted by DuBois et al. Moreover, even subtle spectral features predicted by theory were present in the observations. A generalized depiction of the HFPL spectrum observed at Tromsø and Arecibo versus altitude is shown in Fig. 4 along with a portrayal of the height profile of the HFIL spectrum measured at Tromsø. Enhanced ion line spectra have not yet been measured at Arecibo, but the observations are planned once the new HF facility becomes operational. Experimental details and the specific SLT measurements may be found in the Arecibo and Tromsø papers cited above.

In comparing the Arecibo and Tromsø measurements of SLT the question arises as to how long the HF beam can be turned on and what HF interpulse period is necessary to maintain SSSP or, alternatively, at what average power value do HF-induced irregularities form in the plasma, thus invalidating the requirement for an SSSP. Sulzer and Fejer (1994)

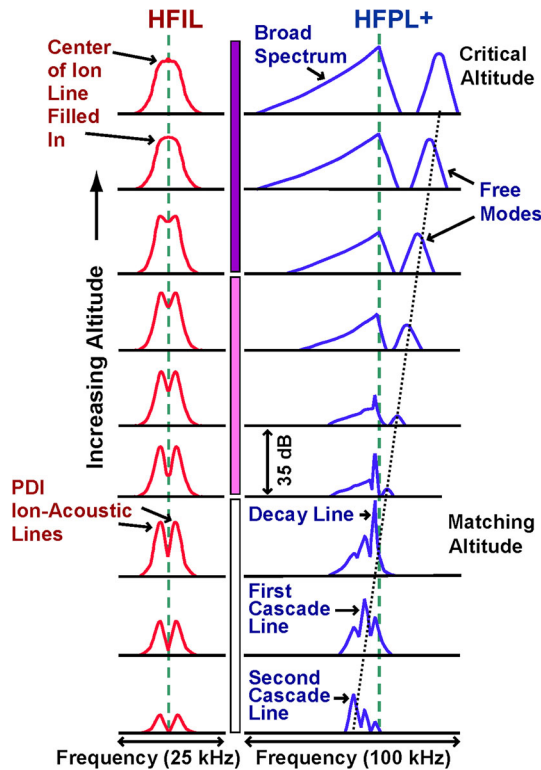


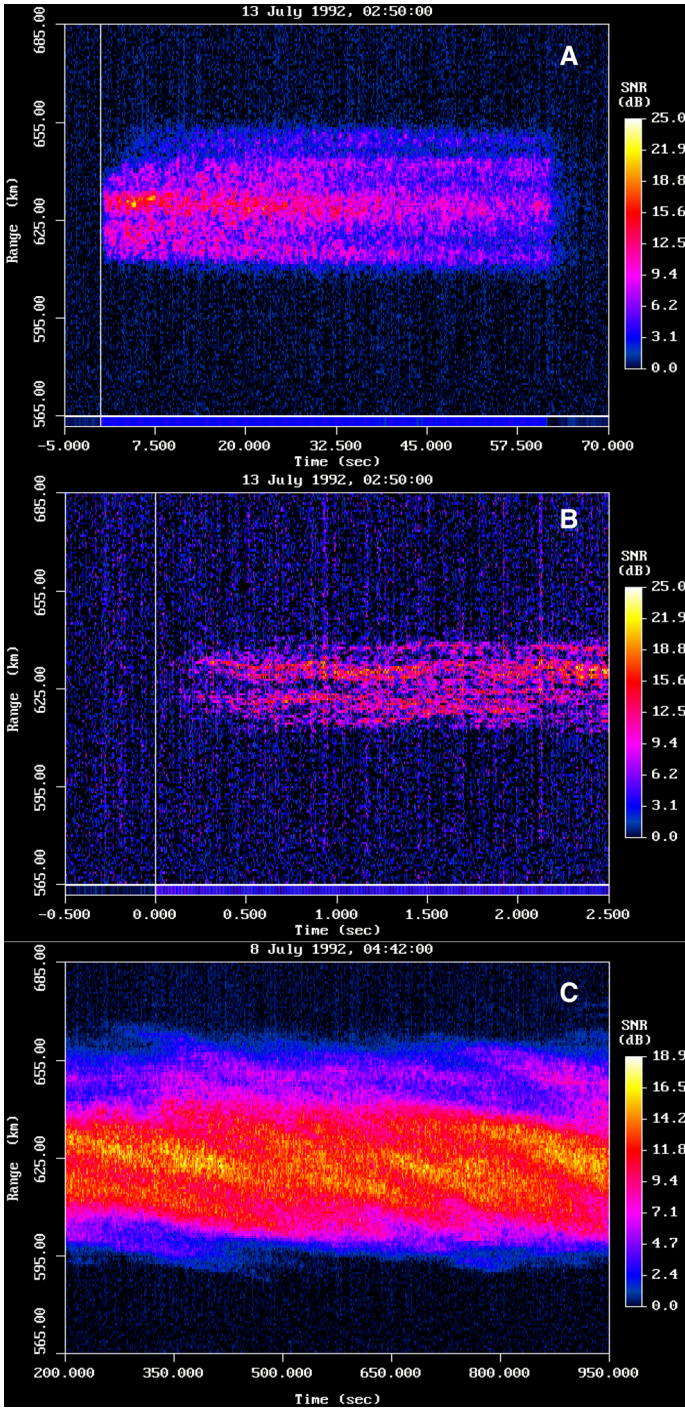
**Fig. 4** Caricature of HFIL spectra (left) and HFPL+ spectra (right) versus height (ordinate) 10–20 ms after HF turn-on in a smooth, stratified, stable plasma. No height values are listed because the total altitude spread of the spectra is dependent on the ionospheric scale height. The nominal separation between altitude bins is 150 m. The dashed green lines correspond to the radar frequency plus  $f_{HF}$  (HFPL+) and the radar center frequency (HFIL). The HFPL– spectrum is not shown, but it is the same as the HFPL+ spectrum except that it is rotated 180° around the dashed green line and positioned at the radar frequency minus  $f_{HF}$ . Spectral power is plotted on a log10 scale; the vertical separation between HFPL+ and HFIL spectral baselines corresponds to a 35 dB power interval. The black dotted line connecting the HFPL free mode frequencies at the baselines represents the LW dispersion curve in the plasma. SLT with caviton formation occurs near the critical altitude (purple bar), and the PDI is detected near the matching altitude (white bar). The magenta bar indicates the region where the PDI and SLT coexist. (Color figure online)



successfully used 5 and 10 ms HF pulses every second, and the ERP of their HF transmissions was  $\sim 40$  MW. They indicated that valid data in an SSSP is limited to transmission pulse lengths of  $\sim 10$  ms, but probably as long as 15–20 ms at 40 MW ERP with an interpulse period of 1 s. After the upgrade of the AO HF facility in 1997, Cheung et al. (2001) made similar measurements and used 5 ms pulses every 2 s and 5 ms every 1 s with an effective radiated power of 80 MW while maintaining an SSSP.

At Tromsø, Rietveld et al. (2000) transmitted an HF pulse 400 ms in length every 9.6 s at an ERP of 240–270 MW. No correction was made for *D* region absorption. In the Tromsø experiment of Djuth et al. (2004) a 100 ms HF pulse was transmitted every 30 s. In this case the ERP corrected for *D* region absorption was  $\sim 58$  MW. Thus, the Tromsø observations were made with much longer pulses than those used at Arecibo, yet the altitude profiles of the HFPL/HFIL spectra were highly organized and clearly a representation of the wave-plasma process in an SSSP. In fact the Tromsø VHF radar beam used in the experiments is very wide (oval 4 km  $\times$  8 km at 270 km altitude) and any significant natural or HF-induced irregularities in the beam would certainly alter the progression of the spectra with altitude. Also, there was no sign of HF-induced or natural irregularities in diagnostic measurements made with an ionosonde, a scintillation receiver that monitored a 250 MHz downlink passing through the modified ionospheric volume (e.g., Basu et al. 1997), and a SEE receiver. The distinguishing characteristic of the Tromsø experiments is that they both were made in the presence of a strong solar-generated *E* region ( $f_oE \sim 3$  MHz), whereas the Arecibo observations were made at evening hours without a strong solar *E* region. The large Pedersen conductivity generated by *E* region ionization at small solar zenith angles slows down the development of field-aligned plasma irregularities generated by instabilities in the *F* region and is unfavorable for the maintenance of natural field-aligned plasma irregularities (e.g., Vickrey and Kelley (1992); Basu et al. 1987; Bhattacharyya 2004). Thus, it appears that the sunlit *E* region may play a role in the length of an HF pulse that can be transmitted while preserving SSSP conditions.

Daytime ionospheric modification experiments have been conducted at AO with the aid of a chirped-radar technique Birkmayer et al. (1986), Birkmayer and Hagfors (1986), Isham et al. (1987), Isham and Hagfors (1993). These observations show that the LWs detected in the sunlit *F* region are confined to a narrow altitude region near the critical layer. Approximately 40 MW maximum ERP was radiated in these experiments, and the measurements were made near solar minimum. The detected HF-induced LWs were apparently trapped in 3–5 % depletions in electron density. On occasion HF-induced small-scale irregularities are evident in these data, but the irregularity amplitudes are not large enough to alter the altitude of the HF-enhanced LWs. Missing from the chirp observations are the large (factor of 50) fluctuations in HFPL power over minute time scales arising from thermal self-focusing of the HF wave in the plasma and PDI waves seen with standard HFPL spectral and power measuring techniques (e.g., Kantor 1974; Carlson and Duncan 1977; Duncan and Behnke 1978; Showen and Kim 1978; Farley et al. 1983). Many of the standard measurements were made under sunlit conditions both at solar minimum and at solar maximum. The thermal self-focusing creates kilometer-scale irregularities across **B** (e.g., Duncan and Behnke 1978), and an AE satellite over flight of AO revealed  $n_e$  perturbations of 1–3 % at an HF reflection height of 260 km (Farley et al. 1983). Certainly a 3 %  $n_e$  depletion due to thermal self-focusing would be evident in the chirped-radar data and would influence the height of the HFPL, but this is not seen. In part, the chirped-radar results may be indicative of low HF electric fields in the *F* region. *D* region absorption combined with a maximum ERP of only 40 MW along with additional damping of LWs by photoelectrons give rise to a relatively weak HF pump wave. In addition, the presence of a





◀ **Fig. 5** HF-induced 3-m AFAIs measured with a 49.92 MHz radar positioned on the island of Antigua. In **a** the temporal evolution of the 3-m AFAIs is shown for a 1-min HF transmission into an initially, cold, unmodified *F* region plasma. An expanded view of the data in **(a)** at HF turn-on is presented in **(b)**. The blue bar at the bottom of the two panels indicates the time interval when the HF beam was on, and vertical white lines designate the exact time when the HF beam was turned on. The late-time development of AFAIs after 20 min of HF transmissions is displayed in **(c)**. Note that the data in **(a)** were acquired on a different day than the data in **(c)**. (Color figure online)

conducting solar *E* layer makes the structuring of the *F* region plasma more difficult. At this point it is clear that the daytime HFPL measurements obtained with the chirped-radar technique are not the same as the results obtained during evening/nighttime hours.

### 3 Development of the HFPL and HFIL over Intermediate Time Scales

Intermediate time scales cover the range from  $\sim 15\text{--}40$  ms to  $20\text{--}90$  s after HF turn-on. All measurements presented in this section were made under evening/nighttime conditions. One important advantage of such observations at AO is that *D* region absorption of the pump wave no longer exists, and the HF wave has a direct path to the *F* region except in the case of sporadic *E* when  $f_oE_s \geq f_{HF}$ . The absence of *D* region absorption is particularly important in experiments conducted under solar minimum conditions when low ( $\sim 4\text{--}5$  MHz) HF frequencies must be used because of low  $f_oF_2$  values. After  $\sim 15\text{--}40$  ms of HF transmissions in the nighttime environment at AO, the nature of the wave-plasma interaction begins to change because of the formation of HF-induced irregularities in the plasma. Over time scales of  $\sim 15\text{--}40$  ms to  $\sim 20$  s following HF turn-on, horizontally stratified irregularities (e.g., Fejer et al. 1984) and short-scale (1–20 m) artificial AFAIs are generated in the Arecibo *F* region. It is believed that these irregularities play a key role in the HFPL behavior over intermediate time scales.

An example of backscatter from HF-induced 3-m AFAIs is provided in Fig. 5. These AFAI data were acquired with a 49.92 MHz radar deployed on the island of Antigua. The 49.92 MHz antenna consisted of four rows of 26 half-wave dipoles. The vertical and horizontal two-way beamwidths were  $\sim 10^\circ$  and  $\sim 2^\circ$ , respectively. Because of the well-known aspect sensitivity of the AFAI backscatter the radar was pointed perpendicular to geomagnetic field lines in the Arecibo *F* region to optimize the signal return. During the experiment the Arecibo HF beam was tilted  $12^\circ$  from vertical in the direction of geographic north. The radar beam was set at an elevation angle of  $\sim 21^\circ$  and was directed toward the ionospheric location of peak HF power density at 250 km altitude. The transmitted pulse width was 6.7  $\mu\text{s}$ , which yielded a range resolution of 1 km.

Figure 5a illustrates the development of 3-m AFAIs in a “cold” background ionosphere. Prior to HF turn-on, the Arecibo HF beam had been turned off for 12 min. The Arecibo HF frequency was set to 5.1 MHz, and approximately 30 MW ERP was transmitted for a 1-min interval. The range resolution of the data is 1 km. Figure 5b shows an expanded view of the HF turn-on in Fig. 5a. The initial range extent of the 49.92 MHz radar echo in Fig. 5b corresponds to the lateral size of the radar beam width (22 km) at the location of the HF beam. Thus, the HF beam half-power width at reflection ( $\sim 33$  km) is wider than the radar beam. In Fig. 5a the echo range increases as the AFAI intensity increases across the HF beam and AFAIs extend further up and down geomagnetic field lines. One important aspect of these observations is the relatively short period of time required to detect 3-m AFAI after HF turn-on in a cold ionosphere. In Fig. 5b the first radar

echoes emerge above the noise background within 140 ms of HF beam turn-on. This time (140 ms) represents an upper limit on the time period required to generate significant HF-induced electron density perturbations in the plasma.

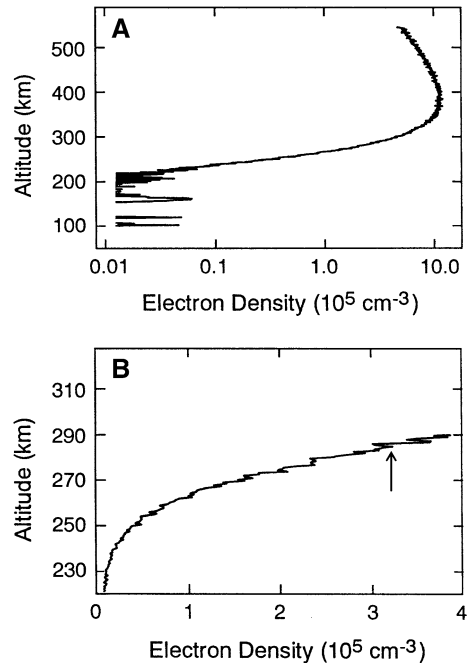
In other tests conducted with the Antigua radar, it was found that AFAI scatter can be detected after a cold turn-on of the HF beam at only 4 MW ERP. These measurements were made on July 8, 1992. The HF beam was turned off for 18 min prior to the turn-on at 4 MW ERP. This detection threshold is somewhat less than the value of 12.8 MW reported by Noble and Djuth (1990) for a Guadeloupe AFAI field site. The discrepancy arises in part because of the greater sensitivity of the Antigua radar to AFAIs brought about by its reduced range to the modified volume. The Antigua radar range to the center of the HF beam was  $\sim 625$  km versus  $\sim 730$  km for Guadeloupe. The  $(\text{range})^{-4}$  dependence of backscatter power gives rise to a factor of  $\sim 1.9$  improvement in radar sensitivity at Antigua. In addition, a better aspect geometry may have also contributed to increased sensitivity at Antigua.

It should be noted that the 4 MW ERP detection threshold is so low as to rule out AFAI production caused solely by the thermal parametric instability (e.g., Grach et al. 1977, 1978a, b; Das and Fejer 1979). A comparison of theoretical thresholds is provided by Noble et al. (1987). Noble and Djuth (1990) show that the detection threshold for AFAIs is close to that of the Arecibo HFPL. This suggests a different scenario for AFAI generation. Intense Langmuir oscillations produced by strong turbulence and/or parametric decay processes invariably lead to the formation of small-scale electron density perturbations via the ponderomotive force. These irregularities can subsequently be reinforced by LW self-focusing in the plasma. AFAIs initially driven near the region of HF reflections could then penetrate into the region of the upper hybrid resonance and trigger so-called resonance instabilities (e.g., Vas'kov and Gurevich 1975, 1977; Inhester et al. 1981; Inhester 1982). Thus, ionospheric irregularities initially driven by intense Langmuir oscillations at higher heights could provide "seed" irregularities for AFAIs. On the other hand, AFAIs initially driven directly near the upper hybrid resonance level will diffuse up and down geomagnetic field lines. If these irregularities penetrate to heights near HF reflection, they will greatly impact LW propagation in the plasma and may alter the production of Langmuir turbulence.

Repeatable HFPL results are obtained only with the cold turn-on of the HF beam in an SSSP plasma. With the aid of AE satellite data, one can define an evening/nighttime SSSP in the  $F$  region above Arecibo as a plasma with small-scale (less than 2 km) fluctuations of less than  $\pm 0.2$  % over lateral distances of 10's of kilometers at a given altitude. This does not include large-scale secular changes in the  $F$  region resulting from gradual lateral  $n_e$  gradients. A stable ionosphere refers to the fact that the vertical layer motion is minimal ( $<10$  m/s) and that the dynamics of geomagnetic storms are absent. Moreover, conditions suitable to the development of very large HF-induced temperatures and temperature gradients (e.g., Djuth et al. 1987b; Newman et al. 1988; Duncan et al. 1988; Djuth 1989; Hansen et al. 1992; González et al. 2005) are assumed not to be present. The above conditions are usually satisfied in the evening/nighttime  $F$  region at Arecibo.

The general characteristics of Langmuir turbulence excited in an  $F$  region under evening/nighttime conditions are totally repeatable provided that a cold start is conducted in the SSSP environment. This cold turn-on condition is satisfied by turning the HF beam off for an extended period of time (10–15 min) allowing residual irregularities to  $\mathbf{E} \times \mathbf{B}$  drift outside of the HF beam prior to a 1-min HF transmission. Background ionospheric measurements are made during a period immediately before HF beam turn-on. Figure 6 shows the background  $n_e$  profile made just before HF turn-on during the evening of 3 May 1990.

**Fig. 6** Electron density profile recorded prior to the cold HF turn-on at 21:10:00 AST on 3 May, 1990 (a) and expanded view of *bottomside F* region gradient (b). The arrow indicates the point of HF reflection (286 km altitude) for a 5.1 MHz wave ( $n_e = 3.2 \cdot 10^5 \text{ cm}^{-3}$ )



These data were obtained near the maximum of solar sunspot cycle 22. The electron density profile of Fig. 6 was measured during a 3-min period (21:06:50 AST–21:09:50 AST) prior to the turn-on of the HF beam at 21:10:00 AST. In this case,  $f_oF2$  was 9.4 MHz, and the modification frequency was 5.1 MHz. The former corresponds to a maximum plasma density of  $1.09 \times 10^6 \text{ cm}^{-3}$ ; whereas the 5.1 MHz modification wave reflects at a “critical altitude” ( $\sim 286 \text{ km}$ ) corresponding to an electron density of  $3.2 \times 10^5 \text{ cm}^{-3}$ . The ionosphere scale length  $H$  is measured to be  $29.2 \pm 1.2 \text{ km}$  at the critical altitude. In addition, the background electron and ion temperatures were measured during the background measurement period of Fig. 6 using the Arecibo multiple radar autocorrelation function observing program (Sulzer 1986b). The results obtained near the critical altitude were  $T_e = T_i = 943 \pm 4 \text{ K}$ .

High-resolution measurements of LW and ion wave power versus altitude are presented in Fig. 7 for the full 1-min HF pulse following the cold turn-on along with a temporal expansion of the first 5.6 s of modification. The observational format is similar to that of Djuth et al. (1990), but the spatial resolution is  $\sim 3.5$  times better. The Arecibo 430 MHz radar was operated in an “impulse” mode; a low-power pulse  $\sim 0.5 \mu\text{s}$  (or slightly less) in length was transmitted within an interpulse period of 730  $\mu\text{s}$ . The receivers at the two plasma line channels ( $430 \text{ MHz} \pm f_{HF}$ ) and ion line channel (430 MHz) each had a bandwidth of 2 MHz. All three receiver channels were simultaneously monitored. The data streams were oversampled to facilitate interpolation over spatial scales less than 75 m (the resolution dictated by the 0.5  $\mu\text{s}$  pulse). All data were oversampled at range gates separated by 0.125  $\mu\text{s}$ , yielding a sample spacing of 18.75 m. For the measurements, the 430 MHz radar beam was pointed toward the center of the HF modification volume in the F region above the Isote HF facility. The zenith angle and azimuth of the radar beam were  $3.5^\circ$  and  $33^\circ$ , respectively. No HF transmissions were made for 12 min prior to turn-on of the HF

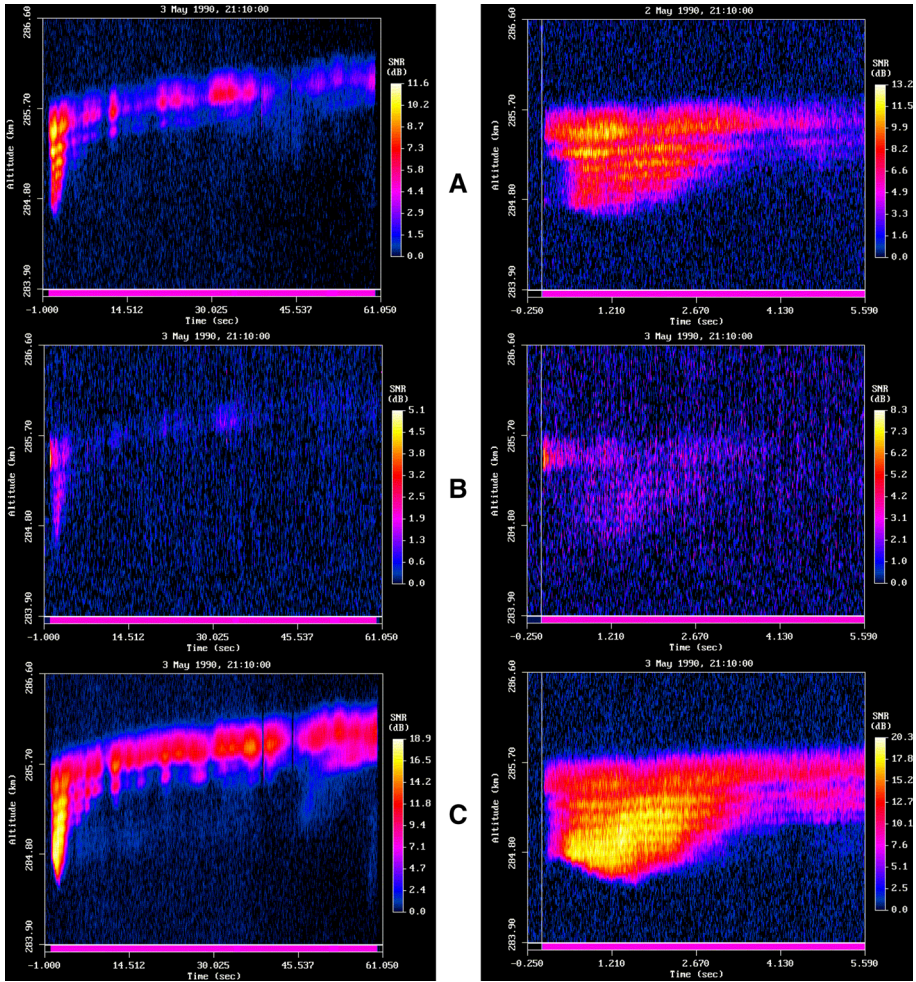


**Fig. 7** High altitude-resolution measurements of the HFPL+ (*top a*), HFIL (*middle b*) and the HFPL– (*bottom c*) versus time after cold HF turn-on at 21:10:00 AST on 3 May 1990. Signal strength is expressed as a signal-to-noise ratio (SNR). The panels on the right are a more detailed view of the first 5.6 s of the HF modifications shown on the *left*. The *panels* on the *right* highlight the downward extensions of the radar echoes. A *magenta bar* at the *bottom* is used to indicate the time interval when the HF beam was on. *This bar* is *black* when the HF beam is off. The *vertical white lines* in the *panels* on the *right* designate the exact time when the HF beam is turned-on. (Color figure online)

beam in Fig. 7. The HF beam was turned on for the one-min transmission of Fig. 7 and then turned off in preparation for the next “cold” turn-on of the HF wave in the plasma. The transmitted HF power was 40 MW ERP. Note that corrections for relative antenna gain at the upshifted/downshifted plasma lines and the ion line were not made because these parameters were not available for this experiment. Shen and Brice (1973) reported model values for conditions that existed in 1972. Over the course of 18 years the height of the line feed gradually sank relative to its ideal focused position above the Arecibo dish thereby changing the 430 MHz antenna gain curve (see e.g. Djuth et al. 1994). No

calibrations were made during the interim period. However, at the time of the current experiment it was known that the downshifted plasma line had significantly more gain than the upshifted plasma line.

In Fig. 8, an annotated version of the downshifted plasma line data of Fig. 7c is shown along with the ionospherically reflected HF wave simultaneously measured at AO. In these observations, the first detection of the HFPLs/HFIL echoes above the noise level occurs  $\sim 13$  ms after HF turn-on rather than within 2 ms in similar measurements reported by Djuth et al. (1990). Other more sensitive measurements made by integrating coded long-pulse data (e.g., Sulzer and Fejer 1994) indicate that the HFPL echo becomes visible within 1 ms of turn-on in a cold background ionosphere. The reason for this lies in the trade-off between altitude resolution and system sensitivity. In the case of the short-pulse measurements both were made using receivers having bandpasses of 2 MHz. However, the earlier measurements employed radar pulses that were 1.5  $\mu$ s in length rather than 0.5  $\mu$ s. With very short pulses, the Arecibo radar never develops its full peak power output. The measurements presented here have temporal integration of 17 pulses, which is insufficient to overcome the adverse impact of reduced transmitter power when signals are weak.

The strongest HFPL echoes in Fig. 8b and the strongest HF-enhanced ion-line (HFIL) echoes in Fig. 7b initially occur at the first maximum of the HF standing wave pattern (1st SWM) in the plasma. Over a time scale of  $\sim 1$  s, HFPL echoes become evident at six additional maxima in the standing wave pattern at lower heights and five maxima in the case of the HFIL. The downward extension of the echo in altitude and its retreat back to higher altitudes is part of the HFPL “overshoot process.” This terminology is adopted from the work of Showen and Kim (1978). After the overshoot, the echoes of Fig. 8a are initially detected at the first four maxima in the standing wave pattern, then at three maxima, then at two maxima, and then at only the first maximum with the occasional appearance of the second maximum for the first  $\sim 45$  s. At late times (20–90 s) after a cold HF turn-on at a power level of  $\sim 40$  MW ERP, the HFPL echo breaks up into patches as large scale (1–2 km) packets of irregularities develop. The spatial phase of the initial HF-induced irregularity packet relative to the radar beam (830 m in diameter) is random which

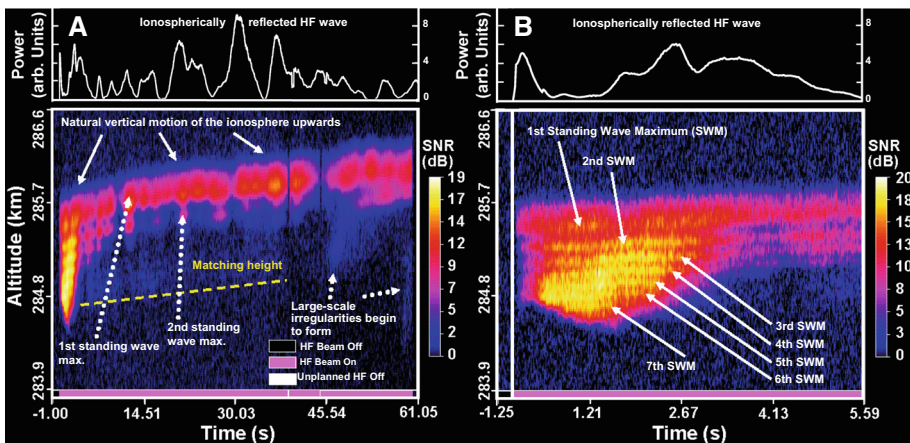


**Fig. 8** Bottom of Fig. 7 (HFPL–) with detailed annotations and plots of the power of the ionospherically reflected modifying HF wave received using the Arecibo 305 m dish. An “unplanned HF off” refers to the loss of half of the HF transmitter array which reduces the HF power density by a factor of four



accounts for the 70 s variation in observed onset time. The large-scale irregularities are presumably caused by the thermal self-focusing instability (e.g., Perkins and Valeo 1974), which also leads to the filamentation of the HF beam. The 430 MHz radar detects HFPLs in the large-scale structures as they  $\mathbf{E} \times \mathbf{B}$  drift through the beam. The beginning of the breakup process is evident in Fig. 8a at  $\sim 45$  s following HF turn on and near the end of the 60 s transmission period at the downshifted HFPL. Notice also how the echo at the 2nd SWM begins to smear out at  $\sim 52$  s and that the weak echo below reflection at 60 s begins to extend downward in altitude. A better view of the breakup is provided in Djuth et al. (1990), and an example with extended HF transmissions is included in discussions below. Small gaps in the HFPL echoes evident near 39 and 44 s relative time are caused by the brief loss of transmissions from half of the HF antenna array. During these periods, antenna arcing triggers a detection circuit which automatically shuts down part of the antenna array, and the transmitted ERP is reduced by a factor of four.

Except for the exact time delay of the HFPL breakup, the development of the induced turbulence illustrated in Figs. 7 and 8 is typical of all other measurements made at Arecibo in a cold background ionosphere under nighttime conditions. However, the absolute power of the HFPL can vary by 1.0–1.5 dB throughout a nighttime run. Most likely this is related to changes in HFPL altitude, changes in  $H$ , or variations in the output power of the HF transmitter. The 5.6 s data segment in Fig. 8b clearly reveals the presence of horizontal stratifications in the HFPL data. Weaker stratifications are also discernible in the HFIL backscatter. Notice that during the overshoot process (first  $\sim 3$  s following HF turn-on) the strongest echoes at the downshifted HFPL are lower in height than those at the upshifted HFPL. This is a consistent feature of the cold turn-on morphology. It is interesting to note that this altitude asymmetry is the reverse of what would be expected if LWs having a broad wavenumber spectrum propagated freely up and down the interaction region. In the case of freely propagating waves in an SSSP, the strength of the upshifted HFPL would tend to increase with decreasing height, whereas the downshifted HFPL would be strongest near the 1st SWM. In Fig. 7, strong ion-line backscatter is observed only for a brief (150 ms) period following HF turn-on. HFIL echoes tend to be strongest near the 1st SWM. However, the HFIL participates in the overshoot process as is evident in the downward extension of the weakened HFIL echo, and its retreat to the 1st SWM. The HFIL also exhibits peaks at the standing wave maxima similar to the HFPL.

The time history of the reflected HF wave in Fig. 8 reveals only random fading of the signal caused by the  $\mathbf{E} \times \mathbf{B}$  drift of natural irregularities and perhaps HF-induced large-scale irregularities at late times ( $>45$  s after HF turn-on) having scale sizes of one or more (i.e.  $n$ ) Fresnel zones ( $\sim 5.4\sqrt{n}$  km diameter) near the point of HF reflection. There is no sign that significant absorption of the HF wave by AFAIs at the upper hybrid resonance is responsible for the overshoot. If this were true, the HF signal would be greatly suppressed beginning  $\sim 3$  s after HF turn-on as it is at Tromsø (Fejer and Kopka 1981). Moreover, Fejer et al. (1989) shows that the reflected HF transmissions at 5.13 MHz exhibit very little attenuation during periods of a strong overshoot. Similarly, Noble and Djuth (1990) show that 3-m FAIs and HFPLs are excited with no sign of significant absorption of the ionospherically reflected HF wave. Thus, while AFAIs may play a role in the overshoot, it is not through the anomalous absorption of the HF pump wave by the AFAIs.

Figure 9 shows an “altitude slice” of the observations presented in Fig. 7 for a 17 pulse (36.5 ms) integration period beginning 2.300 s after HF turn-on. In this figure, simultaneous measurements at the upshifted and downshifted HFPL are plotted along with the theoretically calculated standing wave pattern of the modifying HF wave assuming no

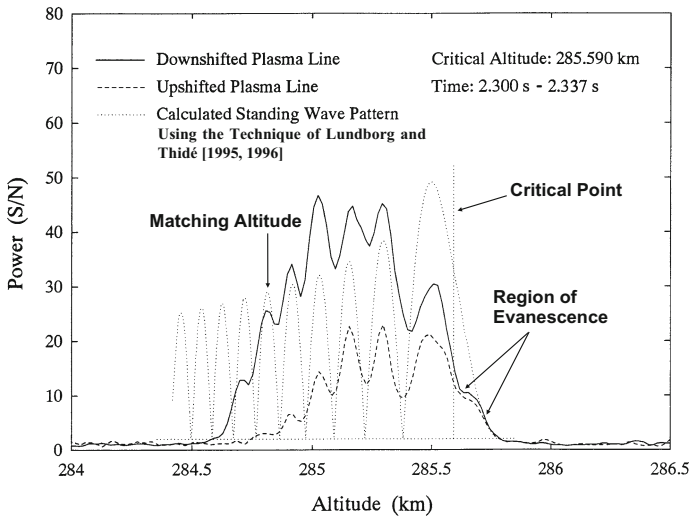


**Fig. 9** HFPL+ and HFPL− power expressed as a SNR versus altitude for the slice of Fig. 7 data from 2.300 to 2.337 s after HF turn-on. The HFPL peaks closely follow the calculated HF standing wave pattern. Note that a region of evanescence is evident above the critical point (point of HF reflection). The matching altitude corresponds to the altitude at which the AO 430 MHz radar should detect the PDI

absorption of the pump wave in the plasma. As noted above, in the nighttime  $F$ -region the assumption of low absorption for a  $f_{HF} = 5.1$  MHz pump wave is a very good one. The standing wave pattern was calculated for the Arecibo geomagnetic field geometry using an accurate approximation to the full wave solution (Lundborg and Thidé 1985, 1986; Thidé and Lundborg 1986). This pattern was fit to the downshifted HFPL observations allowing the scale length  $H$  and the critical altitude (where  $f_{pe} = f_{HF}$ ) to vary as free parameters. The scale length determines the absolute separation between maxima in the standing wave pattern, but the relative separation is not strongly dependent on  $H$ . In this particular example, the deduced value of  $H$  is  $28.9 \pm 0.8$  km. This compares well with the estimate of  $29.2 \pm 1.2$  km obtained from the incoherent scatter electron density profile of Fig. 6.

Overall, the peaks in HFPL backscatter conform to the maxima in the standing wave pattern. The exact match is rather striking. Because of the limited altitude resolution of the measurements ( $\sim 75$  m), the minima do not approach the zero power level. This would be expected if very little collisional or anomalous absorption were present. Notice that in the region of HF wave evanescence above the critical altitude, there is a distinctive bump in upshifted/downshifted HFPL power. This bump is commonly observed in the data.

In Fig. 10, four altitude slices are presented to illustrate the early time evolution of the radar echoes after HF turn-on. Within the first 37 ms of HF turn-on, the HFIL is strongly present in the data, but the HFPLs are barely detectable. The results indicate that at HF turn-on there is a transient increase in the HFIL power. This is similar to the Tromsø observations of Djuth et al. (2004). Between 0.037 and 0.073 s, the upshifted/downshifted HFPL and the HFIL are strongly excited at the 1st SWM. From Fig. 9, one finds that the first maximum is near 285.5 km. After 0.073 s the HFPL echoes quickly spread to lower altitudes, but the detected HFILs are mostly confined to the 1st SWM. Very weak HFPL excitation is present at the matching altitude near 284.7 km. This is the altitude at which the  $k$ -matching condition for the radar and LWs/oscillations is satisfied in the plasma for

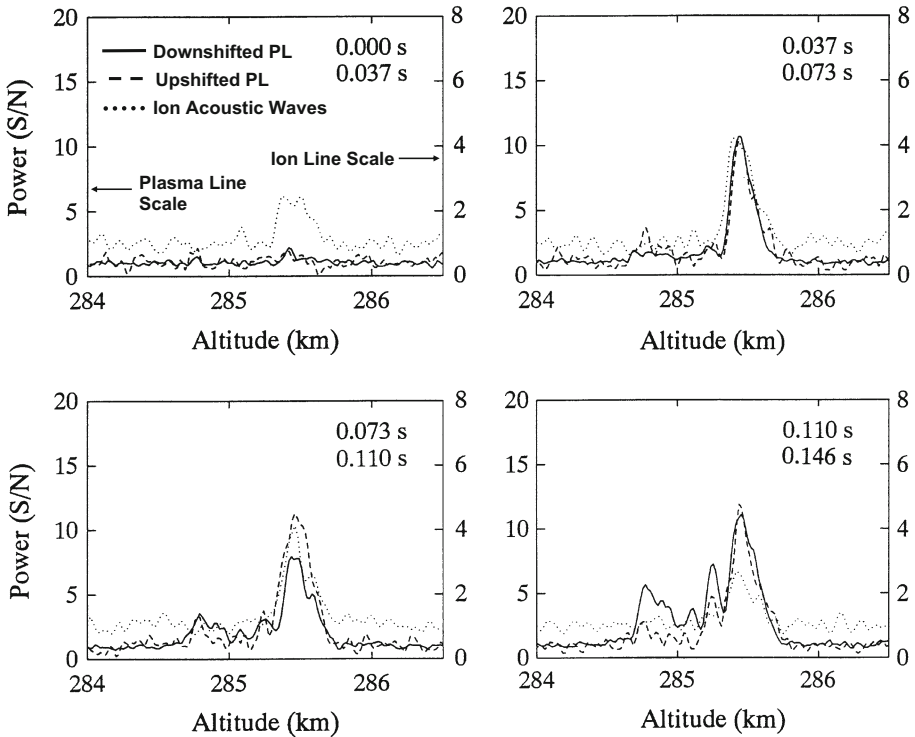


**Fig. 10** Altitude slices of HFPL and HFIL power at four times following HF turn-on in Fig. 7

the PDI. (See Sect. 1; Eq. 1; Fig. 1.) Spectral observations made at the matching height at very early times after HF turn-on are reported by Fejer et al. (1991), Sulzer and Fejer (1994) and Cheung et al. (2001). The observed spectral signals are much stronger than the radar power results shown here. In part this is because of the lack of sensitivity endemic to the short-pulse technique. However, reasonably strong signals are evident in Fig. 9 at 2.300 s after HF turn-on, which is the time at which the HFPL reaches its nadir altitude during the overshoot. After the overshoot the HFPL at the matching height is barely detectable in Figs. 7 and 8 until the HFPL begins to expand downward in altitude because of large-scale irregularity formation by thermal self-focusing.

#### 4 The HFPL and HFIL at Late Times in the Modification Process

As noted above at late times  $>20\text{--}90$  s after HF turn-on the HFPL echo begins to break up because of the thermal self-focusing. An example of a cold turn-on sequence with HF transmissions lasting more than 3 min is presented in Fig. 11. The HF frequency was 5.1 MHz and 40 MW ERP was transmitted. The HF beam was turned off for 20 min prior to the cold turn-on. In this case, the initiation of the HFPL break-up at  $\sim 57$  s after HF turn-on is similar to that of Figs. 7 and 8. The observed break-up of the HFPL into patches is part of the cold-start evolutionary path and is observed 100 % of the time at evening/nighttime hours with 40 MW ERP. However, the detailed structuring of the HFPL echoes



in altitude and the temporal evolution of the patches is always different. It is therefore not surprising that HFPL spectral measurements performed in the past in this environment were not repeatable. At evening/nighttime hours, repeatable results are only achieved with the cold start scenario discussed earlier. At late-times, the large-scale modification environment is populated by a discrete number of kilometer-scale field-aligned structures (e.g., Duncan and Behnke 1978). Large-scale ( $\sim 3$  km) “packets” of smaller-scale AFAIs were observed in the rocket measurements of Kelley et al. (1995). Each packet contained filamentary irregularities having spatial scales across the geomagnetic field  $\mathbf{B}$  of  $\sim 1\text{--}14$  m; the separation between individual filaments is  $\sim 15$  m. The irregularities take the form of depletions in  $n_e$  having a mean depth of  $\sim 6\%$  with a range of depths of

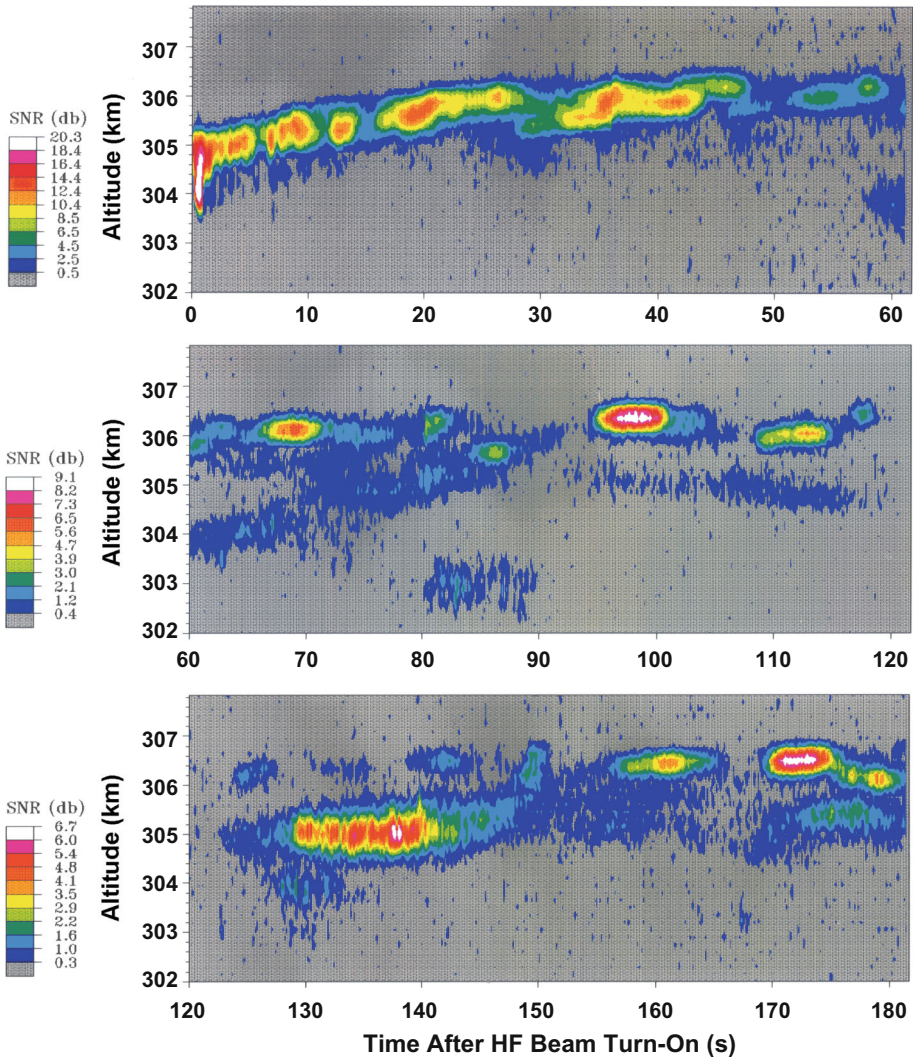


**Fig. 11** High altitude-resolution measurements of the HFPL— versus time after a cold HF turn-on at 21:50:00 AST on 29 April 1988. The altitude resolution is 225 m. Signal strength is expressed as a SNR

2–14 %. The HFPL patches seen in Fig. 11 can be interpreted in terms of LW propagation inside these packets. Most likely the LW propagation is similar to that described by Muldrew (1978a).

Scans of the HF modified volume with the AO radar were performed to achieve a better understanding of the HFPL patches. A typical result is presented in Fig. 12. In this case, continuous HF transmissions were made beginning 10 min prior to the observations shown. During this observation, the frequency of the HF transmissions was 5.1 MHz and  $\sim 40$  MW ERP was transmitted. The radar beam was positioned at a zenith angle of  $3.5^\circ$ ; the azimuth sweep started at  $163^\circ$  (19:59:45 AST), moved through center of the HF beam at 270 km altitude ( $33^\circ$  azimuth) at 20:05:30 AST, and arrived at  $270^\circ$  azimuth at 20:10:25 AST. Beginning at  $163^\circ$  azimuth, the 430 MHz radar scans across the southeast quadrant of the HF beam on its northward path through the center of the HF beam ( $33^\circ$  azimuth). Thereafter, the radar line-of-sight moves nearly east–west across the northwest quadrant of the HF beam. After reaching the geographic north position ( $0^\circ$  azimuth) at 20:07:00 AST, the beam moves west–southwest as it scans towards  $270^\circ$  azimuth.

In Fig. 12a, the increase in average plasma line altitude with time is caused by the natural movement of the ionosphere upwards. Note, however, that regions of HFPL scatter are highly structured. The detected Langmuir turbulence is believed to reside in large-scale ( $\sim 1\text{--}3$  km) “packets” of geomagnetic AFAIs. Ducted propagation (Muldrew 1978a) allows HFPL backscatter to be detected over an extended altitude interval (2–3 km). Given the measured scale length  $H = 29.2$  km near the point of HF reflection, field-aligned perturbations with an  $n_e$  depth of  $\sim 3\text{--}11$  % relative to the background profile would produce the observed altitude spread in the HFPL. This is similar to the range of  $\sim 2\text{--}14$  % obtained with rocket-borne instruments (Kelley et al. 1995). Essentially, the Langmuir turbulence “paints” the field-aligned structures in which it resides. Separations between the  $n_e$  structures in Fig. 11a range from 0.9 to 2.3 km, which is smaller than those measured by Kelley et al. (1995). Figure 12b shows an expanded view of the Langmuir turbulence as the 430 MHz radar beam passes near the center of the HF modified volume. The HFPL patches of highly structured backscatter are not unlike those illustrated in Fig. 11 above.

Additional evidence for the presence of packets of filamentary irregularities at Arecibo is embedded in the Rayleigh fading statistics of the 49.92 MHz AFAI backscatter measured from Antigua. Data acquired with the Antigua radar in the late time environment are shown in Fig. 5c. The Rayleigh fading is brought about by the presence of a limited

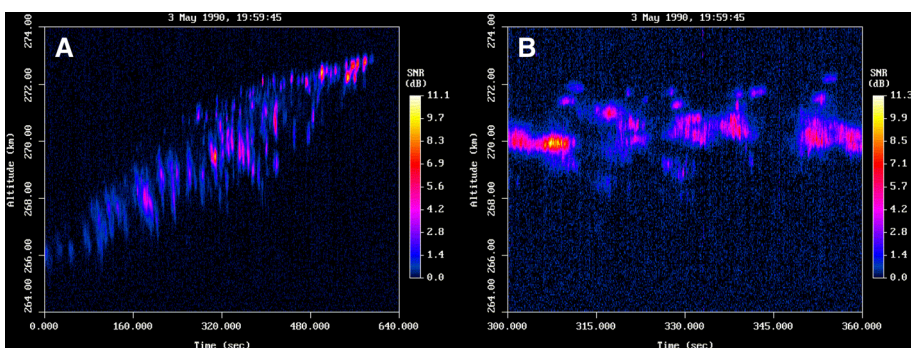


**Fig. 12** HFPL- power measured as the 430 MHz radar beam scans across the HF-modified ionospheric volume (a). Temporal expansion of the echoes in (a) near the center of the HF beam in the ionosphere (b)

number of scattering centers within a radar range cell that most likely corresponds to the packets of filamentary irregularities seen in the rocket experiment of Kelley et al. (1995). The tilted structures in Fig. 5c are caused by large-scale scatterers moving across the HF beam. Individual scattering centers cannot be resolved in RTI plots of this nature because the wavefront of the 49.92 MHz beam encompasses most of the HF beam. However, future experiments that make use of a VHF radar interferometer would be useful in resolving individual scatterers.

In Fig. 13 simultaneously recorded HFPL and HFIL power spectra obtained in a HFPL patch are displayed versus altitude with 150 m altitude resolution. These data were acquired with the coded long-pulse technique (Sulzer 1986a). During this experiment the modifying HF frequency was 5.1 MHz, and 30 MW ERP was transmitted. The radar measurements were made in a heavily conditioned plasma. Prior to the measurements the HF beam was on continuously for 4 h, and this operational mode was continued throughout the observation period. The scale length  $H$  was measured to be 41 km during the observations. The observed echo spread of 3.30 km is consistent with the presence of HF-induced electron density perturbations of the order of 8 %. Each spectrum appears to be an amalgamation of the SLT spectra and the PDI spectra shown in Fig. 4. In fact, the diffuse HFPL spectra underlying the cascade lines in Fig. 13 resemble the broad spectra generated by caviton collapse. This is in stark contrast to measurements made within  $\sim 10$  ms of HF turn-on at Arecibo. In the SSSP environment, all spectral features predicted by theory are

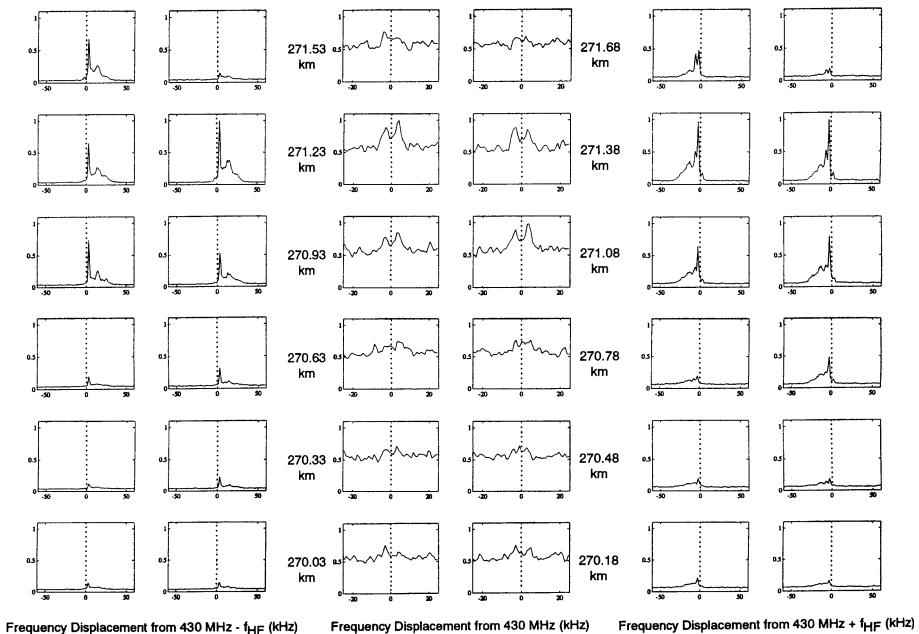


**Fig. 13** HFPL– ( $430 \text{ MHz} - f_{\text{HF}}$ ), HFIL ( $430 \text{ MHz}$ ), and HFPL+ ( $430 \text{ MHz} + f_{\text{HF}}$ ) spectra versus altitude in a heavily preconditioned plasma. The radar measurements were made on 12 July 1992, and the display is the average of data from 05:03:12 AST to 05:04:18 AST. The ordinate corresponds to spectral power plotted on a linear scale. Two column pairs are shown for each resonance line. The altitudes indicated for the HFIL apply to each of the two plasma lines. Data from lower altitudes (268.23–269.88 km) are omitted because the spectral shapes are the same as those at 268.23 km above, and their power values taper to zero at 268.23 km

present in an orderly progression with altitude in the Arecibo observations (Fejer et al. 1991; Sulzer and Fejer 1994; Cheung et al. 2001). This implies that the excitation process proceeds differently in presence of AFAIs and that the radar  $\mathbf{k}$ -matching condition changes when HF-excited LWs and IAWs are viewed in AFAIs. As ionospheric ducts develop, waves excited at small angles relative to  $\mathbf{B}$  propagate into the radar field-of-view (Muldrew and Showen 1977; Muldrew 1978a, 1985, 1991, 1992). Thus, LWs generated at different lateral locations and altitudes can propagate into the radar range cell (a cylinder  $\sim 780$  m in diameter and 150 m in range) if they have the proper  $\mathbf{k}$  vector for detection by the radar. The focus of the above work is on LW propagation in ducts having dimensions of 25–80 m across geomagnetic field lines.

Mjølhus et al. (2001) present a theory of PDI in the presence of short-scale magnetic field-aligned ducts. In this formalism, the parametric instability decays directly into discrete ducted wave modes in the plasma. The decay instability threshold is found to be slightly higher in the duct and the growth rate is slightly lower compared to an SSSP. Examples are provided for  $\sim 4$  m wide ducts. More importantly, the numerical calculations of Mjølhus et al. (2001) show that the LW energy density is far higher in the duct than outside of it in a homogeneous plasma. Mjølhus et al. (2001) indicate that the total energy injection is higher for the duct modes because energy is injected from the pump field into the Langmuir turbulence through a number of separate instabilities involving competing duct modes, where each instability has a growth rate comparable to that of the homogeneous state outside the duct. They suggest that the inhomogeneous energy distribution inside versus outside the duct points to an alternative driving mechanism for the formation/enhancement of ducts. Higher energy density implies larger local heating, which is due to the corresponding inhomogeneous heating and the resulting transport process may lead to the slow growth of the duct. Note that in Sect. 3 it was proposed based on experimental data that the excitation of LWs might give rise to AFAIs that could serve as “seeds” for upper hybrid instabilities. The generation of cavitons in the presence of short-scale ducts has not, to our knowledge, been studied at the above level although it is feasible to do so. In laser-plasma simulations SLT phenomena are observed to coexist with density striations (Vu et al. 2012).

It is important to remember that the initial HFPL observations at Arecibo (e.g., Kantor 1974) were all made in a highly preconditioned plasma containing AFAIs. The spectral observations were not altitude-resolved, but the altitude-integrated spectral return appeared amenable to interpretations involving parametric decay instabilities in an SSSP plasma. This interpretation is incorrect. Only the spectral results of Fejer et al. (1991), Sulzer and Fejer (1994), and Cheung et al. (2001) satisfy the SSSP condition and their interpretation in terms of the SLT/WLT formalism of DuBois et al. yields excellent agreement with theory. All predicted spectral details are evident in the Arecibo observations.

## 5 Discussion

We have described the development of the HFPL in the Arecibo  $F$  region from 1 ms to 180 s and beyond. The early time HFPL spectra of Sulzer and Fejer (1994) were measured in the evening with HF pulses as long as 50 ms every 1 s. However, as the authors indicated, the valid data in an SSSP is obtained with transmission pulse lengths of  $\sim 10$  ms, but probably pulses up to 15–20 ms can be used at 40 MW ERP with an interpulse period of 1 s. At higher HF power levels of 80 MW ERP (Cheung et al. 2001) 5 ms pulses were transmitted every 2 s to insure SSSP conditions, but experiments were



also conducted with a 5 ms pulse width and a 1 s interpulse period at 80 MW ERP, and an SSSP was preserved. Thermally driven instabilities such as the thermal parametric instability (e.g. Grach et al. 1978b) and the resonance instability (e.g., Vas'kov and Gurevich 1977) at the upper hybrid resonance, and thermal self-focusing (e.g., Duncan and Behnke 1978) respond to the average power set by the HF duty cycle, so increasing the pulse repetition time to  $\sim 4$  s may allow longer HF pulses to be transmitted provided that the  $F$  region is very stable. The motivation behind extending the HFPL measurements in an SSSP is to measure the HFPL spectra up to the point where the "overshoot" begins in the plasma. It is assumed that the overshoot entails the formation of HF-induced electron density irregularities. Also the use of an increased pulse repetition period is an effective means of determining whether irregularities are generated locally as a result of Langmuir turbulence excited over a period of  $>20$  ms. (see Sect. 3.)

The experiments of Sulzer and Fejer (1994) and Cheung et al. (2001) were performed at evening hours when the Pedersen conductivity was relatively small. With the new AO facility it is of interest to perform similar experiments with the HFPL and HFIL during the daytime when the  $E$  region Pedersen conductivity may be large enough to inhibit irregularity growth rates in the plasma and thereby allow longer HF pulses to be transmitted in an SSSP. At the same time, the use of transmissions at 8.175 MHz will mitigate  $D$  region absorption, lower ion Landau damping of the HFIL, and slightly lower the collision damping rate of the HFPL compared to evening/nighttime experiments at 5.1 MHz. In addition, daytime radar measurements involving the coded long-pulse technique could be used to complement the chirped-radar technique Birkmayer et al. (1986), Birkmayer and Hagfors (1986); Isham et al. 1987; Isham and Hagfors 1993) by determining the wideband (250-ÅkHz) high-resolution (1 kHz) LW spectra of the echoes observed with the chirp technique. As noted in Sect. 2.2, the chirp technique indicates that the HFPL is narrowly confined to an altitude region near the critical layer, and additional data is needed to determine how this occurs. In the past, frequency resolution of the chirp technique has been too low (8.9 kHz) to discriminate, for example, between the signatures of the PDI and SLT. A 30 MHz radar looking perpendicular to  $F$  region geomagnetic field lines will also be available during experiments with the new AO HF facility. This will enable HF-induced 5-m short-scale irregularities to be monitored in the  $F$  region above the HF facility during HFPL/HFIL experiments. A comparison between 5-m irregularity volumetric cross sections and growth rates during day and evening/nighttime observations is of great value for the new round of AO investigations.

The modified/extended Zakharov model of DuBois et al. has been successful in predicting the early time HFPL results at Arecibo (Sulzer and Fejer 1994; Cheung et al. 2001). These predictions were made well in advance of the experiments. All HFPL spectral details were found to be consistent with the model. In the Arecibo experiments discussed above the HF electric fields at the first standing wave maximum were  $\sim 1.4$  V/m (40 MW ERP) and  $\sim 2.0$  V/m (80 MW ERP) assuming an  $n_e$  scale length of  $H = 50$  km. However, for high turbulence levels such as those at Tromsø, the Zakharov simulation models may be reaching their limits of applicability. For example, Tromsø results obtained for an electric field of  $\sim 7.9$  V/m at the first standing wave maximum revealed that broadened cascades develop first, followed by narrow cascade peaks that reside on top of the broad structures (Djuth et al. 2004). In addition, suprathermal electrons produced by caviton burn-out recirculate through the production region because of elastic electron collisions that occur outside the region (e.g., Carlson et al. 1982; Gurevich et al. 1985, 2000). According to Carlson et al. (1982), "the suprathermal electrons have a mean free path of several kilometers and suffer about ten elastic collisions before each inelastic collision. No matter

what the acceleration mechanism is, elastic collisions serve to rapidly fill in loss cones.” Thus, a more complete description of the modification process requires that successive turbulent layers be tied together because they are linked by downgoing and upcoming fluxes of suprathermal electrons. This can only be accomplished with a purely kinetic simulation model.

The ubiquitous generation of suprathermal electrons from Langmuir turbulence created by parametric instabilities has led to the development of new kinetic modeling tools which can be applied to HF ionospheric modification phenomena. Considerable progress has been made in laser-plasma modeling. One model called the Quasilinear Zakharov model (QZAK) (Sanbonmatsu et al. 2000a; Myatt et al. 2013; Vu et al. 2014a) can model 10 km or greater plasma layers near HF reflection in 2D simulations and hundreds of meters in 3D simulations with current parallel computing capabilities. Currently there exists 1D, 2D, and 3D versions of QZAK that are directly applicable to HF ionospheric modification, but only the 1D results have been published (Sanbonmatsu et al. 2000a, b). However, in all cases the quasilinear coding is essentially identical for laser and ionospheric applications. The 10 km spatial scale for 2D ionospheric simulations and the corresponding hundreds of meters for 3D simulations is set by the computer resources necessary to perform the calculations. This model has been validated in appropriate regimes by comparison with complete kinetic particle-in-cell simulations (Sanbonmatsu et al. 2000b; Vu et al. 2012, 2014a). Recent work describing hot electrons resulting from SLT excited by the laser-driven two-plasmon decay instability has found that burn-out of collapsing cavitons is the dominant acceleration mechanism. Agreement on this is obtained from both full PIC simulations (Vu et al. 1999, 2012) and the QZAK model (Myatt et al. 2013, Vu et al. 2014a). QZAK has been employed in 2D and 3D simulations with thousands of cavitons in the simulated volume (Vu et al. 2012, 2014b). New caviton diagnostics display the spatial shape, scale, and orientation of the cavitons. Detailed electron velocity distributions and hot electron fluxes are computed. Suprathermal electron “temperatures” 10–100 times the background (Maxwellian) electron temperature are found at normalized turbulence levels comparable to those found in HF heating simulations (Vu et al. 2012, 2014b). The energy carried off by hot electrons leads to a significant decrease in the Langmuir turbulence levels for strong excitation, i.e. for strong HF pumping. Developments in 3D simulation capabilities may also allow the future extension of these models to the case of Langmuir turbulence in the presence of short-scale AFAIs.

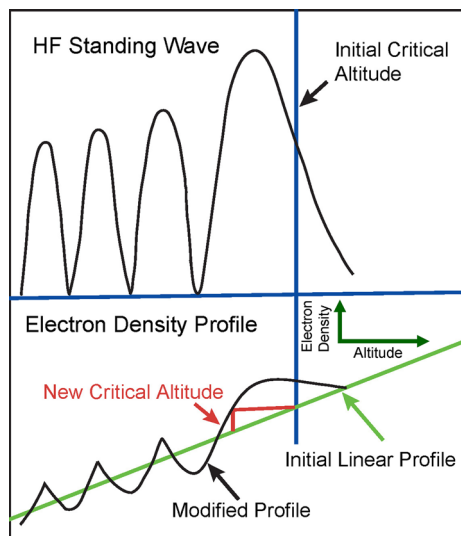
In general the accurate prediction of suprathermal fluxes by QZAK will aid aeronomy calculations of electron transport, electron loss, and electron thermal energy balance in the upper atmosphere. This is an important application that illustrates the spin-off science that is possible with the new HF facility. These studies will also help in validating suprathermal electron models for laser plasma interactions in laser-induced inertial confinement applications. The local determination and resolution of the hot electron velocity distribution possible in the HF heating experiments significantly exceeds any diagnostic currently available for laser applications. In this regard it should be noted that in the scaled variables used in the extended Zakharov modeling the turbulence levels in the laser-plasma applications are of the same order of magnitude as in the HF ionospheric modification applications.

Studies of suprathermal electrons accelerated by HF-induced instabilities have been made in the past at Arecibo using non-resonantly enhanced plasma lines as a diagnostic (e.g., Carlson et al. 1982; Fejer et al. 1985; Fejer and Sulzer 1987; Gurevich et al. 2000). Arecibo radar measurements of plasma lines enhanced by suprathermal electrons are much more sensitive to low-level electron fluxes than, for example, optical observations of

induced airglow. Past observations have shown that suprathermal electrons are present in the late-time modification environment (Carlson et al. 1982; Gurevich et al. 2000) and that there is a transient increase in suprathermal electrons immediately following turn-on of the HF beam (Fejer et al. 1985; Fejer and Sulzer 1987). When the new AO facility becomes operational, suprathermal electrons will be simultaneously monitored using enhanced non-resonant plasma lines and optical emissions from HF-excited resonance lines in O, N<sub>2</sub> and N<sub>2</sub><sup>+</sup>. The plasma line offers an instantaneous wideband measurement of the suprathermal electrons, whereas CCD optics provides the ability to image the modified volume.

An explanation for the HFPL/HFIL overshoot displayed in Figs. 7, 8, 9 and 10 remains elusive. In the past other overshoot data along with several explanations have been put forth to explain the Arecibo results (e.g., Showen and Kim 1978; Duncan and Sheerin 1985; Kuo et al. 1987,1993; Kuo and Lee 1990; Muldrew 1986,1988,1992). Based on overshoot data acquired without cold turn-ons of the HF beam, Duncan and Sheerin (1985) suggest that altitudinal effects associated with the overshoot “may find their explanation in some combination of the theories of soliton formation and collapse, wave ducting, profile modification, parametric instabilities, and associated interactive processes.” The goal of future studies in this area is to sort out the roles of the above processes and identify the mechanisms that are dominant. However, no existing theory fully explains all of the cold turn-on HFPL/HFIL results in Figs. 7 and 8. The current data shows that the overshoot consists of an extension of the HFPL signal downwards in altitude from the 1st SWM to the 7th SWM followed by a retreat back to the first two standing wave maxima at higher altitudes. In Fig. 8b the period of the overshoot extends from ~0.037 to 3.40 s after HF turn-on. During the overshoot the downshifted HFPL is more intense near the bottom of the participating altitude region, whereas the upshifted HFPL is more intense at higher altitudes near the 1st SWM. The peaks in the HFPL echoes versus altitude become well developed and follow the HF standing wave pattern during the interval 0.18–2.74 s. During this period there are some dynamic changes in the relative HFPL amplitudes at the standing wave maxima, but the basic pattern shown in Fig. 9 is nominally representative of other times. The HFIL has a strong transient response near the first maximum in the standing wave pattern lasting for about 0.15 s. Thereafter, the echo intensity follows the standing

**Fig. 14** Illustration of electron density profile modifications resulting from the ponderomotive force exerted by the Langmuir turbulence during the overshoot. The electron density scale length  $H$  is steepened at the new critical altitude of the modified profile



wave pattern with an even distribution of amplitude across the overshoot region. As noted in Sect. 3 anomalous absorption by short-scale AFAIs excited at lower heights cannot be used to explain the overshoot.

One would think that the ponderomotive force  $-\nabla E^2$  exerted by the envelopes of LWs in the standing wave pattern would carve out an electron density perturbation particularly because the LW electric field is much greater than the electromagnetic electric field. A schematic illustration of the corresponding  $n_e$  profile modification is provided in Fig. 14. A similar effect is often observed in laser plasmas, but in that case the ponderomotive force is supplied by the electromagnetic pump wave (e.g., Kruer 2003). This type of profile modification is most likely dynamically unstable and might lead to the end of the overshoot, but it is most likely not responsible for the overshoot. In the past efforts have been made to measure the density perturbations caused by the standing wave pattern under late time conditions (Fejer et al. 1984). However, these measurements were made at low power (10 MW ERP) and the estimated  $\Delta n_e/n_e$  was  $10^{-4}$ . Cavity formation resulting from the caviton cycle or other processes near the 1st SWM where the overshoot process begins is an attractive concept because it accounts for one key feature of the data. However, this alone will not explain the overshoot. It is clear that progress in this area requires that the HFPL/HFIL spectra be measured versus altitude with good (75 m) altitude resolution during and after the overshoot process.

At late times in the modification process, HFPL measurements made with the short-pulse technique have been used to map out the large-scale HF-induced irregularities/structures in the  $F$  region. These results are in general agreement with those measured via rocket (Kelley et al. 1995), satellite overpass (Farley et al. 1983), and HFPL intensity measurements at AO (Duncan and Behnke 1978; Farley et al. 1983). The large-scale irregularity data are generally interpreted theoretically as resulting from thermal self-focusing of the HF pump wave in the ionosphere (e.g., Perkins and Valeo 1974; Craigin and Fejer 1974; Craigin et al. 1977). HF-induced  $F$  region scintillations measured at AO with radio astronomical sources (Basu et al. 1983) reveal similar large-scale irregularities having scale lengths of 1.5–2 km. Also, the scale length decreases by a factor of 1.1 when the HF power increases by a factor of 1.5, which is consistent with the theory of Craigin and Fejer (1974). However, Frey and Duncan (1984) used similar radio-star scintillation techniques at AO and concluded that the large-scale irregularities were  $\sim 600$  m in size or less, which is inconsistent with the work of Craigin and Fejer (1974). Farley et al. (1983) indicate that there are major discrepancies between theory and experiment and that significant improvements in theory are required to explain the observed satellite and HFPL results at AO. The measurements of Kelley et al. (1995) show that the large-scale structures consist of packets of filamentary depletions separated by 1.5–6.0 km. The power spectrum of depletions falls off as  $k^{-4}$  for wavenumbers  $k$  larger than  $0.4 \text{ m}^{-1}$  and remains above the system noise for structures down to 1 m. Thus, the self-focusing process may entail cascades of irregularities, not just the generation of kilometer-scale structures. The hope for the future is that better diagnostic measurements will usher in better theory. For example, ultra high-resolution measurements of electron density perturbations made by applying the CLP technique (Sulzer 1986a) to daytime photoelectron-enhanced plasma lines (Djuth et al. 1994) will add significantly to the knowledge base. Similar nighttime measurements are also possible using conjugate photoelectrons during the winter at AO. In addition  $T_i$ ,  $T_e$ , and  $v_i$  can be sequentially measured along with resonant LWs and IAWs thereby allowing the electron temperature fluctuations and plasma diffusion processes to be monitored. Finally, we note that the availability of a 30 MHz radar interferometer on the island of Guadeloupe will help resolve issues brought forth by Kelley et al. (1995) concerning the embedding of meter-scale geomagnetic AFAIs in packets of filaments.



## 6 Conclusions

In the current work, the evolution of HF-induced LWs/oscillations and ion waves at AO is shown to evolve over three distinct time scales beginning with a cold start in an SSSP. These include early time development (first 15–20 ms after HF turn-on in a cold plasma, perhaps longer), intermediate times ( $\sim 40$ – $100$  ms to  $\sim 20$ – $90$  s), and late times in the modification process  $>20$ – $90$  s. All measurements were made with the Isote HF facility with  $f_{HF} = 5.1$  MHz under evening/nighttime conditions. The early time observations were made both with 40 MW ERP and 80 MW ERP; whereas the intermediate and late time observations were made with 40 MW. The early time data acquired at AO by Sulzer and Fejer (1994) and Cheung et al. (2001) validates the SLT simulations of DuBois et al. as do the Tromsø results of Isham et al. (1999), Rietveld et al. (2000), and Djuth et al. (2004). In the SSSP regime, the linear and nonlinear physics of the HF induced turbulence is well described by the extended Zakharov model. This model has predicted almost all of the observed phenomena under SSSP conditions and can be derived directly from the Vlasov–Maxwell equations (DuBois et al. 1995). In addition, this model has been validated by comparison with fully kinetic simulation models. DuBois et al. [2001] provide a comprehensive description of SLT as it applies to Arecibo.

There is uncertainty with respect to the exact time when the SSSP measurements transition into the overshoot process, but it is probably in the range of 15–40 ms. Here we are assuming that the overshoot entails the formation of HF-induced electron density irregularities in the  $F$  region. The beginning of the overshoot represents the start of the intermediate stage in HFPL development. In the evening/nighttime environment of the observations presented herein, the overshoot is present from  $\sim 37$  ms to 3.40 s, and the peaks in HFPL excitation versus altitude become well-settled and follow the peaks in the HF standing wave pattern during the period  $\sim 0.18$ – $2.74$  s. The HFIL has a strong transient response near the first maximum in the standing wave pattern lasting for about 0.15 s. Thereafter, the echo intensity follows the standing wave pattern with an even distribution of amplitude across the overshoot region. The physical processes involved in the overshoot remain elusive, and currently no theory can comprehensively explain the results presented herein. In the future high-altitude, high frequency resolution spectra will be obtained during the overshoot period to clarify the nature of the LW and IAW turbulence present during the overshoot with emphasis on the spectra present when peaks in the turbulence follow the HF standing wave pattern. After the overshoot, the HFPL echoes retreat back to the first and second maxima of the HF standing wave pattern until thermal self-focusing sets in 20–90 s after HF turn-on. Thereafter the HFPL breaks up into patches. At late times the HFPLs are excited in large-scale electron density structures and the HFPL performs the important task of mapping out the structures.

The boundary of 20–90 s between intermediate times and late times is set by formation of large-scale HFPL patches, which can form either inside the  $\sim 830$  m diameter radar beam or outside of it and subsequently drift into beam. As a result, the boundary is probably closer to 20 s, which is the earliest time that patches are detected inside the radar beam. At late times, the HFPL echo is believed to be the result of LWs propagating in the patches of filamentary irregularities arising from the thermal self-focusing process. The process of irregularity formation is far more complex than originally thought as illustrated by the short-pulse radar scan in this paper and the work of Kelley et al. (1995). It is clear from the earlier work of Farley et al. (1983) that new theoretical initiatives are needed to adequately model the thermal self-focusing process and associated irregularity production.

Daytime measurements made with the chirped-radar technique indicate that LWs reside in electron density depletions near the first HF standing wave maximum (i.e. within  $\sim 200$  m of the critical altitude), and normally there are no echoes at the matching altitudes where the PDI would be detected by the radar (e.g., Isham and Hagfors 1993). The cavity size is estimated to be less than 20 m. These results are fundamentally different than those observed in the evening/nighttime. In part, the daytime results may be the result of a weakened HF pump wave resulting from *D* region absorption. In this case, the thermal self-focusing instability and other thermally driven instabilities may be below threshold. HF, high-altitude resolution HFPL observations are needed to determine the type of instability process at work near the critical altitude (e.g., PDI, SLT).

Arecibo's new HF facility offers opportunities not only to resolve past HFPL issues but also to explore instabilities in a higher HF power regime. In addition, AO now operates with dual radar beams allowing HF-induced suprathermal electron fluxes along **B** to be simultaneously measured above and below the region of Langmuir turbulence at early and late times in the modification process. This arrangement is ideal for testing the prediction of Carlson et al. (1982) that "Any flux initially directed down will produce a steady state flux in both directions, about one-third of the total flux at any level being backscattered up towards the source region." This statement applies to altitudes below  $\sim 300$  km. Alternatively HFPLs/HFILs can be simultaneously measured along with one receiver channel dedicated to measurements of suprathermal electron fluxes. Observations of this type make it possible to test and refine kinetic simulations of HF-induced turbulence (e.g., the QZAK model developed by DuBois et al.). One model prediction is that suprathermal electrons generated by caviton burn-out regulate turbulence levels in the plasma. Accurate predictions of suprathermal fluxes will greatly aid aeronomy studies of electron transport, electron loss, and thermal energy balance in the upper atmosphere. HF-generated suprathermal electron fluxes offer a simple, reliable, and repeatable source flux for studies of the upper atmosphere. In general, one can expect many pioneering investigations to be performed with the new AO facility as spin-offs of the HFPL and related suprathermal electron science.

**Acknowledgments** FTD acknowledges support from the NSF under grants ATM-9529392 and AGS-1012006, and from AFRL under contract F19628-94-C-0101. We thank M. P. Sulzer for his technical assistance during our radar experiments at AO. Discussions with B. Thidé and T. B. Leyser are gratefully acknowledged. DFD acknowledges early support from the LDRD program at Los Alamos National Laboratory and support from NSF including the grants ATM-9503147 and ATM-9713563. Important discussions with H.X. Vu and D. A. Russell are gratefully acknowledged. The Arecibo Observatory is operated by SRI International under a cooperative agreement with the National Science Foundation (AST-1100968), and in alliance with Ana G. Méndez-Universidad Metropolitana, and the Universities Space Research Association.

## References

- S. Basu, E. S. Basu, S. Ganguly, W.E. Gordon, Coordinated study of subkilometer and 3-m irregularities in the F region generated by high power HF heating at Arecibo. *J. Geophys. Res.* **88**, 9217–9225 (1983)
- Sa Basu, E. MacKenzie, Su Basu, E. Costa, P.F. Fougere, H.C. Carlson, H.E. Whitney, 250 MHz/GHz scintillation parameters in the equatorial, polar, and auroral environments. *IEEE Comm.* **SAC-5**(2), 102–115 (1987)
- Sa Basu, E. Costa, R.C. Livingston, K.M. Groves, H.C. Carlson, P.K. Chaturvedi, P. Stubbe, Evolution of subkilometer scale ionospheric irregularities generated by high-power HF waves. *J. Geophys. Res.* **102**, 7469–7475 (1997)

- A. Bhattacharyya, Role of E region conductivity in the development of equatorial ionospheric plasma bubbles. *Geophys. Res. Lett.* **31**, L06806 (2004). doi:[10.1029/2003GL018960](https://doi.org/10.1029/2003GL018960)
- W. Birkmayer, T. Hagfors, W. Kofman, Small-scale plasma-depletions in Arecibo high-frequency modification experiments. *Phys. Rev. Lett.* **57**, 1008–1011 (1986)
- W.T. Birkmayer, T. Hagfors, Observational technique and parameter estimation in plasma line spectrum observations of the ionosphere by chirped I.S. radar. *J. Atmos. Terr. Phys.* **48**, 1009–1019 (1986)
- H.C. Carlson, L.M. Duncan, HF excited instabilities in space plasmas. *Radio Sci.* **12**, 1001–1013 (1977)
- H.C. Carlson, W.E. Gordon, R.L. Showen, High frequency induced enhancements of the incoherent scatter spectrum at Arecibo. *J. Geophys. Res.* **77**, 1242–1250 (1972)
- H.C. Carlson, V.B. Wickwar, G.P. Mantas, Observations of fluxes of suprathermal electrons accelerated by HF excited instabilities. *J. Atmos. Terr. Phys.* **44**, 1089–1100 (1982)
- P.Y. Cheung, A.Y. Wong, T. Tanikawa, J. Santoru, D.F. DuBois, H.A. Rose, D. Russell, Short time scale evidence for strong Langmuir turbulence during heating of the ionosphere. *Phys. Rev. Lett.* **62**, 2676–2679 (1989)
- P.Y. Cheung, D.F. DuBois, T. Fukuchi, K. Kawan, H.A. Rose, D. Russel, T. Tanikawa, A.Y. Wong, Investigation of strong Langmuir turbulence in ionospheric modification. *J. Geophys. Res.* **97**, 10575–10600 (1992)
- P.Y. Cheung, M.P. Sulzer, D.F. DuBois, D.A. Russell, High-power high-frequency-induced Langmuir turbulence in a smooth ionosphere at Arecibo. II. Low duty cycle, altitude-resolved, observations. *Phys. Plasmas* **8**, 802–812 (2001)
- A.J. Coster, F.T. Djuth, R.J. Jost, W.E. Gordon, The temporal evolution of three-meter striations in the modified ionosphere. *J. Geophys. Res.* **90**, 2807–2818 (1985)
- B.L. Craigin, J.A. Fejer, Generation of large-scale field-aligned irregularities in ionospheric modification experiments. *Radio Sci.* **9**, 1071–1075 (1974)
- B.L. Craigin, J.A. Fejer, E. Leer, Generation of artificial spread F by a collisionally coupled purely growing parametric instability. *Radio Sci.* **12**, 273–284 (1977)
- A.C. Das, J.A. Fejer, Resonance instability of small-scale field aligned irregularities. *J. Geophys. Res.* **84**, 6701–6704 (1979)
- A.C. Das, J.A. Fejer, N.J. Martinic, Three-dimensional saturation spectrum of the parametric decay instability. *Radio Sci.* **20**, 813–818 (1985)
- F. T. Djuth, HF-enhanced plasma lines in the lower ionosphere. *Radio Sci.* **19**, 383–394 (1984)
- F.T. Djuth, C.A. Gonzales, H.M. Ierkic, Temporal evolution of the HF-enhanced plasma line in the Arecibo F region. *J. Geophys. Res.* **91**, 12089–12107 (1986)
- F.T. Djuth, R.J. Jost, H.M. Ierkic, M.P. Sulzer, S.T. Noble, Observations of HF-enhanced ion waves in the ionosphere. *Geophys. Res. Lett.* **14**, 194–197 (1987a)
- F.T. Djuth, B. Thidé, H.M. Ierkic, M.P. Sulzer, Large F-region electron-temperature enhancements generated by high-power HF radio waves. *Geophys. Res. Lett.* **14**, 953–956 (1987b)
- F.T. Djuth, Response of the Arecibo ionosphere to large HF-induced electron temperature enhancements. *Adv. Space Res.* **9**(5), 123–131 (1989)
- F.T. Djuth, M.P. Sulzer, J.H. Elder, High resolution observations of HF-induced plasma waves in the ionosphere. *Geophys. Res. Lett.* **17**, 1893–1896 (1990)
- F.T. Djuth, M.P. Sulzer, J.H. Elder, Application of the coded long pulse technique to plasma line studies of the ionosphere. *Geophys. Res. Lett.* **21**, 2725–2728 (1984)
- F.T. Djuth, B. Isham, M.T. Rietveld, T. Hagfors, C. La Hoz, The first 100 ms of HF modification at Tromsø, Norway. *J. Geophys. Res.* **109**, A11307 (2004). doi:[10.1029/2003JA010236](https://doi.org/10.1029/2003JA010236)
- G.D. Doolen, D.F. DuBois, H.A. Rose, Strong Langmuir turbulence and the OTSI. *Phys. Rev. Lett.* **51**, 335–338 (1983)
- G.D. Doolen, D.F. DuBois, H.A. Rose, Nucleation of cavitons in strong Langmuir turbulence. *Phys. Rev. Lett.* **54**, 804–807 (1985)
- D.F. DuBois, M.V. Goldman, Radiation induced instability of electron plasma oscillations. *Phys. Rev. Lett.* **14**, 544–546 (1965)
- D.F. DuBois, M.V. Goldman, Parametrically excited plasma fluctuations. *Phys. Rev.* **164**, 207–222 (1967)
- D.F. DuBois, M.V. Goldman, Nonlinear saturation of parametric instability: basic theory and application to the ionosphere. *Phys. Fluids* **15**, 919–929 (1972)
- D.F. DuBois, H.A. Rose, D. Russell, Power spectra of fluctuations in strong Langmuir turbulence. *Phys. Rev. Lett.* **61**, 2209–2212 (1988)
- D.F. DuBois, H.A. Rose, D. Russell, Excitation of strong Langmuir turbulence in plasmas near critical density: application to HF heating of the ionosphere. *J. Geophys. Res.* **95**, 21221–21272 (1990)
- D.F. DuBois, H.A. Rose, D. Russell, Coexistence of parametric decay cascades and caviton collapse at subcritical densities. *Phys. Rev. Lett.* **66**, 1970–1973 (1991)

- D.F. DuBois, A. Hanssen, H.A. Rose, Comment on “Langmuir turbulence and ionospheric modification” by P. Stubbe, H. Kohl, and M. T. Rietveld. *J. Geophys. Res.* **97**, 15059–15066 (1992)
- D.F. DuBois, A. Hanssen, H.A. Rose, D. Russell, Space and time distribution of HF excited Langmuir turbulence in the ionosphere: comparison of theory and experiment. *J. Geophys. Res.* **98**, 17543–17567 (1993a)
- D.F. DuBois, A. Hansen, H.A. Rose, D. Russell, Excitation of strong Langmuir turbulence in the ionosphere: comparison of theory and observations. *Phys. Fluids* **5**, 2616–2622 (1993b)
- D.F. DuBois, D. Russell, H.A. Rose, Reduced description of strong Langmuir turbulence from kinetic theory. *Phys. Plasmas* **2**, 76–89 (1995)
- D.F. DuBois, D.A. Russell, P.Y. Cheung, M.P. Sulzer, High-power high-frequency-induced Langmuir turbulence in a smooth ionosphere at Arecibo. I. Theoretical predictions for altitude-resolved plasma line radar spectra. *Phys. Plasmas* **8**, 791–801 (2001)
- L.M. Duncan, R.A. Behnke, Observations of self-focusing electromagnetic waves in the ionosphere. *Phys. Rev. Lett.* **41**, 998–1001 (1978)
- L.M. Duncan, J.P. Sheerin, High-resolution studies of the HF ionospheric modification interaction region. *J. Geophys. Res.* **90**, 8371–8376 (1985)
- L.M. Duncan, J.P. Sheerin, R.A. Behnke, Observations of ionospheric cavities generated by high-power radio waves. *Phys. Rev. Lett.* **61**, 239–242 (1988)
- J.V. Evans, Theory and practice of ionosphere study by Thomson scatter radar. *Proc. IEEE* **57**, 496–530 (1969)
- D.T. Farley, C. LaHoz, B.G. Fejer, Studies of the self-focusing instability at Arecibo. *J. Geophys. Res.* **88**, 2093–2102 (1983)
- J.A. Fejer, Ionospheric modification and parametric instabilities. *Rev. Geophys.* **17**, 135–153 (1979)
- J.A. Fejer, Physical processes of ionospheric heating experiments. *Adv. Space Res.* **8**(1), 261–270 (1988)
- J.A. Fejer, Y. Kuo, Structure in the nonlinear saturation spectrum of parametric instabilities. *Phys. Fluids* **16**, 1490–1496 (1973)
- J.A. Fejer, H. Kopka, The effect of plasma instabilities on the ionospherically reflected wave from a high-power transmitter. *J. Geophys. Res.* **86**, 5746–5750 (1981)
- J.A. Fejer, M.P. Sulzer, The HF-induced plasma line below threshold. *Radio Sci.* **19**, 675–682 (1984)
- J.A. Fejer, M.P. Sulzer, Observations of suprathermal electron fluxes during ionospheric modification experiments. *J. Geophys. Res.* **92**, 3441–3444 (1987)
- J.A. Fejer, F.T. Djuth, C.A. Gonzales, Bragg backscatter from plasma inhomogeneities due to a powerful ionospherically reflected radio wave. *J. Geophys. Res.* **89**, 9145–9147 (1984)
- J.A. Fejer, C.A. Gonzales, H.M. Ierick et al., Ionospheric modification experiments with the Arecibo heating facility. *J. Atmos. Terr. Phys.* **47**, 1165–1179 (1985)
- J.A. Fejer, F.T. Djuth, H.M. Ierick, M.P. Sulzer, Simultaneous observations of the enhanced plasma line and the reflected HF wave at Arecibo. *J. Atmos. Terr. Phys.* **51**, 721–725 (1989)
- J.A. Fejer, M.P. Sulzer, F.T. Djuth, Height dependence of the observed spectrum of radar backscatter from HF-induced ionospheric Langmuir turbulence. *J. Geophys. Res.* **96**, 15985–16008 (1991)
- A. Frey, W.E. Gordon, HF produced ionospheric electron density irregularities diagnosed by UHF radio star scintillations. *J. Atmos. Terr. Phys.* **44**, 1101–1111 (1982)
- A. Frey, L.M. Duncan, Simultaneous observation of HF-enhanced plasma waves and HF-wave self-focusing. *Geophys. Res. Lett.* **11**, 677–680 (1984)
- S.A. González, M.J. Nicolls, M.P. Sulzer, N. Aponte, An energy balance study of the lower topside ionosphere using the Arecibo incoherent scatter radar and heating facilities. *J. Geophys. Res.* **110**, A11303 (2005). doi:[10.1029/2005JA011154](https://doi.org/10.1029/2005JA011154)
- W.E. Gordon, R. Showen, H.C. Carlson, Ionospheric heating at Arecibo: first tests. *J. Geophys. Res.* **76**, 7801–7813 (1971)
- S.M. Grach, A.N. Karashtin, N.A. Mityakov, V.O. Rapoport, VYu. Trakhtengerts, Parametric interaction between electromagnetic radiation and ionospheric plasma. *Radiophys. Quantum Electron. Engl. Transl.* **20**, 1254–1258 (1977)
- S.M. Grach, A.N. Karashtin, N.A. Mityakov, V.O. Rapoport, VYu. Trakhtengerts, Theory of the thermal parametric instability in an inhomogeneous plasma. *Sov. J. Plasma Phys. Engl. Transl.* **4**, 737–741 (1978a)
- S.M. Grach, A.N. Karashtin, N.A. Mityakov, V.O. Rapoport, VYu. Trakhtengerts, Thermal parametric instability in an inhomogeneous plasma (nonlinear theory). *Sov. J. Plasma Phys. Engl. Transl.* **4**, 742–747 (1978b)
- A.V. Gurevich, Y.S. Dimant, G.M. Milikh, V.V. Vas'kov, Multiple acceleration of electrons in the regions of high-power radio-wave reflection in the ionosphere. *J. Atmos. Terr. Phys.* **47**, 1057–1070 (1985)

- A.V. Gurevich, H.C. Carlson, G.M. Milikh, K.P. Zybin, F.T. Djuth, K.M. Groves, Suprathermal electrons generated by the interaction of a powerful radio wave with the ionosphere. *Geophys. Res. Lett.* **27**, 2461–2464 (2000)
- J.D. Hansen, G.J. Morales, L.M. Duncan, G. Dimonte, Large-scale HF-induced ionospheric modifications: experiments. *J. Geophys. Res.* **97**, 113–122 (1992)
- A. Hanssen, Resonance broadening modification of weak plasma turbulence theory. *J. Geophys. Res.* **96**, 1867–1871 (1991)
- A. Hanssen, E. Mjølhus, D.F. DuBois, H.A. Rose, Numerical test of the weak turbulence approximation to ionospheric Langmuir turbulence. *J. Geophys. Res.* **97**, 12073–12091 (1992)
- E. Helmersen, E. Mjølhus, A semikinetic model for ionospheric Langmuir turbulence. *J. Geophys. Res.* **99**, 17623–17629 (1994)
- B. Inhester, Thermal modulation of the plasma density in ionospheric heating experiments. *J. Atmos. Terr. Phys.* **44**, 1049–1059 (1982)
- B. Inhester, A.C. Das, J.A. Fejer, Generation of small-scale field aligned irregularities in ionospheric heating experiments. *J. Geophys. Res.* **86**, 9101–9106 (1981)
- B. Isham, T. Hagfors, Observations of the temporal and spatial development of induced and natural plasma lines during HF modification experiments at Arecibo using chirped incoherent scatter radar. *J. Geophys. Res.* **98**, 13605–13625 (1993)
- B. Isham, W. Birkmayer, T. Hagfors, W. Kofman, Observations of small-scale plasma depletions in Arecibo heating experiments. *J. Geophys. Res.* **92**, 4629–4637 (1987)
- B. Isham, C. La Hoz, T.B. Leyser, M.T. Rietveld, T. Hagfors, Cavitating Langmuir turbulence observed during high-latitude ionospheric wave interaction experiments. *Phys. Rev. Lett.* **83**, 2576–2579 (1999)
- I.J. Kantor, High frequency induced enhancements of the incoherent scatter spectrum at Arecibo, 2. *J. Geophys. Res.* **79**, 199–208 (1974)
- M.C. Kelley, T.L. Arce, J. Salowey, T. Armstrong, M. Carter, L.M. Duncan, Density depletions at the ten-meter scale induced by the Arecibo heater. *J. Geophys. Res.* **100**, 17367–17376 (1995)
- W.L. Kruer, *The Physics of Laser Plasma Interactions (Frontiers in Physics)* (Westview Press, Colorado, 2003), p. 182
- W.L. Kruer, E.J. Valeo, Nonlinear evolution of the decay instability in a plasma with comparable electron and ion temperatures. *Phys. Fluids* **16**, 675–684 (1973)
- S.P. Kuo, M.C. Lee, Temporal evolution of HF-Enhanced plasma lines. *Geophys. Res. Lett.* **17**, 2209–2212 (1990)
- S.P. Kuo, M.C. Lee, A source mechanism producing HF-induced plasma lines (HFPLS) with up-shifted frequencies. *Geophys. Res. Lett.* **19**, 249–252 (1992)
- S.P. Kuo, M.C. Lee, On the generation of a broad downshifted spectrum of HF wave enhanced plasma lines in the ionospheric heating experiments. *Geophys. Res. Lett.* **26**, 3289–3292 (1999)
- S.P. Kuo, B.R. Cheo, M.C. Lee, The role of parametric decay instabilities in generating ionospheric irregularities. *J. Geophys. Res.* **88**, 417–423 (1983)
- S.P. Kuo, M.C. Lee, F.T. Djuth, A new interpretation of plasma-line overshoot phenomena. *Geophys. Res. Lett.* **14**, 961–964 (1987)
- S.P. Kuo, J. Huang, M.C. Lee, On the altitude of the HF-enhanced plasma lines. *J. Geophys. Res.* **98**, 11671–11676 (1993)
- M.C. Lee, J.A. Fejer, Theory of short-scale field aligned density striations due to ionospheric heating. *Radio Sci.* **13**, 893–899 (1978)
- M.C. Lee, S.P. Kuo, Excitation of upper hybrid waves by a thermal parametric instability. *J. Plasma Phys.* **30**, 463–478 (1983)
- M.C. Lee et al., Laboratory reproduction of Arecibo experimental results: HF wave-enhanced Langmuir waves. *Geophys. Res. Lett.* **24**, 115–118 (1997)
- B. Lundborg, B. Thidé, Standing wave pattern of HF radio waves in the ionospheric reflection region, 1. General formulas. *Radio Sci.* **20**, 947–958 (1985)
- B. Lundborg, B. Thidé, Standing wave pattern of HF radio waves in the ionospheric reflection region, 2. Applications. *Radio Sci.* **21**, 486–500 (1986)
- J.F. Myatt, H.X. Vu, D.F. DuBois, D.A. Russell, J. Zhang, R.W. Short, A.V. Maximov, Mitigation of two-plasmon decay in direct-drive inertial confinement fusion through the manipulation of ion acoustic and Langmuir wave damping. *Phys. Plasmas* **20**, 052705 (2013)
- E. Mjølhus, E. Helmersen, D.F. Dubois, Significance of short-scale irregularities for radar diagnostics of HF-driven Langmuir turbulence in the ionosphere. *J. Geophys. Res.* **106**, 18525–18542 (2001)
- G.J. Morales, A.Y. Wong, J. Santoru, L. Wang, Dependence of plasma line enhancement on HF pulse length and ionosphere preconditioning. *Radio Sci.* **17**, 1313–1320 (1982)

- D.B. Muldrew, The role of field-aligned ionization irregularities in the generation of the HF-induced plasma line at Arecibo. *J. Geophys. Res.* **83**, 2552–2560 (1978a)
- D.B. Muldrew, Langmuir wave propagation and the enhanced plasma line in sporadic E. *J. Geophys. Res.* **83**, 5207–5211 (1978b)
- D.B. Muldrew, An ionization duct explanation of some plasma line observations with a 46.8-MHz radar and with a 430-MHz radar. *J. Geophys. Res.* **90**, 6662–6666 (1985)
- D.B. Muldrew, Numerical simulation of the temperature, electron density, and electric field distributions near the ionospheric reflection height after turn-on of a powerful HF wave. *J. Geophys. Res.* **91**, 4572–4580 (1986)
- D.B. Muldrew, Duct model explanation of the plasma line overshoot observed at Arecibo. *J. Geophys. Res.* **93**, 7598–7604 (1988)
- D.B. Muldrew, Duct-model explanation of the broad component of plasma-line spectra observed at Arecibo. *Geophys. Res. Lett.* **18**, 2289–2292 (1991)
- D.B. Muldrew, Initial duct growth determined from cold-start plasma-line data recorded at Arecibo. *Geophys. Res. Lett.* **19**, 65–68 (1992)
- D.B. Muldrew, R.L. Showen, Height of the HF-enhanced plasma line at Arecibo. *J. Geophys. Res.* **82**, 4793–4804 (1977)
- A.L. Newman, H.C. Carlson, G.P. Mantas, F.T. Djuth, Thermal response of the F-region ionosphere for conditions of large HF-induced electron-temperature enhancements. *Geophys. Res. Lett.* **15**, 311–314 (1988)
- D.L. Newman, R.M. Winglee, P.A. Robinson, J. Glanz, M.V. Goldman, Simulation of the collapse and dissipation of Langmuir wave packets. *Phys. Fluids B* **2**, 2600–2611 (1990)
- D.R. Nicholson, M.V. Goldman, Cascade and collapse of Langmuir waves in two dimensions. *Phys. Fluids* **21**, 1766–1776 (1978)
- D.R. Nicholson, G.L. Payne, R.M. Downie, J.P. Sheerin, Soliton versus parametric instabilities during ionospheric heating. *Phys. Rev. Lett.* **52**, 2152–2155 (1984)
- K. Nishikawa, Parametric excitation of coupled waves I. General formulation. *J. Phys. Soc. Jpn* **24**, 916–922 (1968a)
- K. Nishikawa, Parametric excitation of coupled waves I. General formulation. *J. Phys. Soc. Jpn* **24**, 1152–1158 (1968b)
- S.T. Noble, F.T. Djuth, R.J. Jost, W.E. Gordon, Å. Hedberg, B. Thidé, H. Derblom, R. Boström, E. Nielsen, P. Stubbe, H. Kopka, Multiple frequency radar observations of high-latitude E region irregularities in the HF modified ionosphere. *J. Geophys. Res.* **92**, 13613–13627 (1987)
- S.T. Noble, F.T. Djuth, Simultaneous measurements of HF-enhanced plasma waves and artificial field-aligned irregularities at Arecibo. *J. Geophys. Res.* **95**, 15195–15207 (1990)
- G.L. Payne, D.R. Nicholson, R.M. Downie, J.P. Sheerin, Modulational instability and soliton formation during ionospheric heating. *J. Geophys. Res.* **89**, 10921–10928 (1984)
- G.L. Payne, D.R. Nicholson, M.-M. Shen, Numerical test of weak turbulence theory. *Phys. Fluids B* **9**, 1797–1804 (1989)
- F.W. Perkins, A theoretical model for short-scale field-aligned plasma density striations. *Radio Sci.* **9**, 1065–1070 (1974)
- F.W. Perkins, E.J. Valeo, Thermal self-focusing of electromagnetic waves in plasmas. *Phys. Rev. Lett.* **32**, 1234–1237 (1974)
- F.W. Perkins, C. Oberman, E.J. Valeo, Parametric instabilities and ionospheric modification. *J. Geophys. Res.* **79**, 1478–1496 (1974)
- M.T. Rietveld, B. Isham, H. Kohl, C. La Hoz, T. Hagfors, Measurements of HF enhanced plasma and ion lines at EISCAT with high altitude resolution. *J. Geophys. Res.* **105**, 7429–7439 (2000)
- D.A. Russell, D.F. DuBois, H.A. Rose, Collapsing caviton turbulence in one dimension. *Phys. Rev. Lett.* **56**, 838–842 (1986)
- D.A. Russell, D.F. DuBois, H.A. Rose, Nucleation in two-dimensional Langmuir turbulence. *Phys. Rev. Lett.* **60**, 581–584 (1988)
- D.A. Russell, D.F. DuBois, H.A. Rose, Nonlinear saturation of stimulated Raman scattering in laser hot spots. *Phys. Plasmas* **6**, 1294 (1999)
- K.Y. Sanbonmatsu, H.X. Vu, B. Bezzerides, D.F. DuBois, The effect of kinetic processes on Langmuir turbulence. *Phys. Plasmas* **7**, 1723–1731 (2000a)
- K.Y. Sanbonmatsu, H.X. Vu, D.F. DuBois, B. Bezzerides, Quantitative comparison of reduced-description particle-in-cell and quasilinear-Zakharov models for parametrically excited Langmuir turbulence. *Phys. Plasmas* **7**, 2824–2841 (2000b)
- J.S. Shen, N. Brice, Near-field gain calibration for large spherical antennas. *IEEE Trans. Antennas Propag* **AP-21**, 787–792 (1973)

- J.P. Sheerin, J.C. Weatherall, D.R. Nicholson, G.L. Payne, M.V. Goldman, P.J. Hanson, Solitons and ionospheric modification. *J. Atmos. Terr. Phys.* **44**, 1043–1048 (1982)
- R.L. Showen, The spectral measurement of plasma lines. *Radio Sci.* **14**, 503–508 (1979)
- R.L. Showen, D.M. Kim, Time variations of HF-induced plasma waves. *J. Geophys. Res.* **83**, 623–628 (1978)
- V.P. Silin, Parametric resonance in a plasma. *Sov. Phys. JETP Engl. Transl.* **21**, 1127–1132 (1965)
- R.A. Sprague, J.A. Fejer, Simultaneous excitation of parametric decay cascades and of the OTSI in 1D numerical simulations based on Zakharov's equations. *J. Geophys. Res.* **100**, 23959–23972 (1995)
- A.J. Stocker, T.R. Robinson, T.B. Jones, Observations of the effects of ionospheric heating on the amplitude of low-power diagnostic radio waves at Arecibo. *J. Geophys. Res.* **97**, 6315–6322 (1992)
- M.P. Sulzer, A radar technique for high range resolution incoherent scatter autocorrelation function measurements utilizing the full power of klystron radars. *Radio Sci.* **21**, 1033–1040 (1986a)
- M.P. Sulzer, A phase modulation technique for a sevenfold statistical improvement in incoherent scatter data-taking. *Radio Sci.* **21**, 737–744 (1986b)
- M.P. Sulzer, J.A. Fejer, Simultaneous observations of 46.8-MHz and 430-MHz radar backscatter from HF-induced ionospheric Langmuir turbulence. *J. Geophys. Res.* **96**, 17891–17895 (1991)
- M.P. Sulzer, J.A. Fejer, Radar spectral observations of HF-induced ionospheric Langmuir turbulence with improved range and time resolution. *J. Geophys. Res.* **99**, 15035–15050 (1994)
- M.P. Sulzer, H.M. Ierkcic, J.A. Fejer, R.L. Showen, HF-induced ion and plasma line spectra with two pumps. *J. Geophys. Res.* **89**, 6804–6812 (1984)
- M.P. Sulzer, H.M. Ierkcic, J.A. Fejer, Observational limitations on the role of Langmuir cavitons in ionospheric modification experiments at Arecibo. *J. Geophys. Res.* **94**, 6841–6854 (1989)
- B. Thidé, Stimulated scattering of large amplitude waves in the ionosphere: experimental results. *Phys. Scr* **T30**, 170–180 (1990)
- B. Thidé, B. Lundborg, Structure of HF pump in ionospheric modification experiments: linear treatment. *Phys. Scr.* **33**, 475–479 (1986)
- B. Thidé, Å. Hedberg, J.A. Fejer, M.P. Sulzer, First observations of stimulated electromagnetic emission at Arecibo. *Geophys. Res. Lett.* **5**, 369–372 (1989)
- B. Thidé, F.T. Djuth, H.M. Ierkcic, T.B. Leyser, Evolution of Langmuir turbulence and stimulated electromagnetic emissions excited with a 3-MHz pump wave at Arecibo. *J. Geophys. Res.* **100**, 23887–23899 (1995)
- V.V. Vas'kov, A.V. Gurevich, Nonlinear resonant instability of a plasma in the field of an ordinary electromagnetic wave. *Sov. Phys. JETP Engl. Transl.* **42**, 91–97 (1975)
- V.V. Vas'kov, A.V. Gurevich, Resonance instability of small-scale plasma perturbations. *Sov. Phys. JETP Engl. Transl.* **46**, 487–494 (1977)
- E.J. Valeo, C. Oberman, F.W. Perkins, Saturation of the decay instability for comparable electron and ion temperatures. *Phys. Rev. Lett.* **30**, 1035–1038 (1972)
- J.F. Vickrey, M.C. Kelley, The effects of a conducting *E* layer on classical *F* region cross-field diffusion. *J. Geophys. Res.* **87**, 4461–4466 (1992)
- H.X. Vu, B. Bezzerides, D.F. DuBois, ASPEN: a fully kinetic reduced-description particle-in-cell model for simulating parametric instabilities". *J. Comput. Phys.* **156**, 12–19 (1999)
- H.X. Vu, D.F. DuBois, D.A. Russell, J.F. Myatt, Hot electron production by 'cavitating' Langmuir turbulence in the nonlinear stage of the two-plasmon decay instability. *Phys. Plasmas* **19**, 102708 (2012)
- H.X. Vu, D.F. DuBois, D.A. Russell, J.F. Myatt, J. Zhang, Nonlinear development of the two-plasmon decay instability in three dimensions". *Phys. Plasmas* **21**, 042705 (2014)
- H.X. Vu, D.F. DuBois, D.A. Russell, J.F. Myatt, J. Zhang, *Three-dimensional quasilinear, extended, Zakharov nonlinear modeling*, *Phys. Plasmas*, submitted (2014b)
- J.G. Wang, G.L. Payne, D.F. DuBois, H.A. Rose, One dimensional simulations of Langmuir collapse in a radiation driven plasma. *Phys. Plasmas* **1**, 2531–2537 (1994)
- J.G. Wang, D.L. Newman, M.V. Goldman, Vlasov simulations of electron heating by Langmuir turbulence near the critical altitude in the radiation-modified ionosphere. *J. Atmos. Sol. Terr. Phys.* **59**, 2461–2472 (1997)
- J.C. Weatherall, J.P. Sheerin, D.R. Nicholson, G.L. Payne, M.V. Goldman, P.J. Hansen, Solitons and ionospheric heating. *J. Geophys. Res.* **87**, 823–832 (1982)
- V.E. Zakharov, Collapse of Langmuir waves. *Sov. Phys. JEPT Eng. Transl.* **35**, 908–920 (1972)